ELSEVIER

Chemical Geology 195 (2003) 131–157

CHEMICAL GEOLOGY
INCLUDING
ISOTOPE GEOSCIENCE

www.elsevier.com/locate/chemgeo

Contrasting sulfur geochemistry and Fe/Al and Mo/Al ratios across the last oxic-to-anoxic transition in the Cariaco Basin, Venezuela

Timothy W. Lyons[a,*], Josef P. Werne[b,1], David J. Hollander[b,2], R.W. Murray[c]

[a] *Department of Geological Sciences, University of Missouri, 101 Geological Science Bldg., Columbia, MO 65211, USA*
[b] *Department of Geological Sciences, Northwestern University, Evanston, IL 60208, USA*
[c] *Department of Earth Sciences, Boston University, Boston MA 02215, USA*

Received 26 May 2001; received in revised form 22 March 2002

Abstract

An abrupt transition from oxic to anoxic–sulfidic (euxinic) marine bottom waters occurred in the Cariaco Basin in response to increasing productivity resulting from the late Pleistocene post-glacial rise in sea level and corresponding increase in surface-water nutrient availability. The microlaminated sediments of the euxinic interval, which span the last ~ 14.5 ky, suggest a predominance of water-column (syngenetic) pyrite formation based on (1) high pyrite sulfur (S_{py}) concentrations in the surficial sediment layers, (2) values for degree-of-pyritization (DOP) that generally do not increase appreciably with increasing burial, (3) ratios of total iron (Fe_T) to Al that are elevated above the continental baseline recorded in the underlying oxic sediments, and (4) S_{py} isotope trends that largely mimic the $\delta^{34}S_{HS^-}$ of the modern water column. Intermediate DOP values in the microlaminated deposits and Fe_T/Al ratios that are slightly above continental levels indicate an iron reservoir controlled by scavenging during syngenetic pyrite formation in combination with intermediate rates of Fe-bearing siliciclastic accumulation. As predicted from the relative rates of siliciclastic delivery, Fe_T/Al and DOP data lie between end-member values observed in the modern Black Sea. As viewed broadly, Fe_T/Al and DOP relationships in euxinic sediments reflect the balance between syngenetic Fe scavenging and temporal and spatial gradients in siliciclastic input.

Pyrite concentrations are generally low in the underlying oxic marine deposits because of limitations in the supply of organic carbon (C_{org}). However, the upper 80 cm of the Fe-rich, C_{org}-poor, bioturbated sediment show evidence for a strong diffusional HS^- overprint from the overlying, Fe-limited euxinic marine environment. This post-glacial transition manifests in pyrite overprints that are strongly ^{34}S-depleted relative to those in restricted, presently euxinic marine settings elsewhere in the world, such as the Black Sea, where the sedimentary sequence spanning the last glacial–interglacial transition begins with a shift from freshwater to C_{org}-poor oxic marine deposition and thus dominantly sulfate diffusion.

Trends for Mo/Al ratios in the microlaminated sediments suggest that Mo is enriched by roughly two orders of magnitude above the continental levels recorded in the oxic deposits. Organic matter plays a role by enhancing HS^- production and/or by providing a substrate for Mo scavenging. Significant Mo enrichment via diffusion into the upper portion of the bioturbated zone was not observed despite HS^--rich pore waters as recorded in the heavy iron sulfide overprint. We have

* Corresponding author. Tel.: +1-573-882-6328; fax: +1-573-882-5458
E-mail address: lyonst@missouri.edu (T.W. Lyons).
[1] Currrent address: Large Lakes Observatory and Department of Chemistry, University of Minnesota-Duluth, Duluth, MN 55812, USA.
[2] Current address: Department of Marine Sciences, University of South Florida, St. Petersburg, FL 33701, USA.

doi:10.1016/S0009-2541(02)00392-3

not, however, proven that high sulfide concentrations within the water column are required for enhanced Mo sequestration in sediments.

Keywords: Sulfur isotopes; Pyrite; Iron; Molybdenum; Redox history; Cariaco Basin

1. Introduction

With an approximately 580-ky record of alternating oxic and anoxic conditions on glacial–interglacial time scales (Haug et al., 1998; Peterson et al., 2000; Yarincik et al., 2000a,b), the Cariaco Basin provides an ideal natural laboratory for comparative investigations of the biogeochemical cycling of sulfur and redox-sensitive trace metals. In particular, the transition from the oxically deposited sediments of the last glacial episode to the anoxic–sulfidic (euxinic) conditions that have persisted in the water column over the last ~ 14.5 ky is marked by an abrupt juxtaposition of disparate geochemical properties with approximately 6.5 m of organic- and sulfur-rich, microlaminated sediment overlying bioturbated, organic-deficient clay.

The burial of pyrite sulfur (S_{py}) and the related organic-carbon (C_{org}) pathways have long been investigated in modern marine basins (Goldhaber and Kaplan, 1974; Berner, 1982, 1984; Calvert and Karlin, 1991; Lin and Morse, 1991; Middelburg, 1991; Lyons and Berner, 1992; Hurtgen et al., 1999) to refine paleoenvironmental reconstructions over a range of spatial and temporal scales (Raiswell and Berner, 1985, 1986; Anderson et al., 1987; Leventhal, 1987; Dean and Arthur, 1989; Arthur and Sageman, 1994; Werne et al., 2002). The Cariaco Basin, with all its complexity and temporal variability, adds an essential piece to this puzzle.

A variety of trace-element methods have also been developed in recent decades to address paleoredox conditions in ancient black shale sequences (see reviews by Arthur and Sageman, 1994; Jones and Manning, 1994; Wignall, 1994; Schieber et al., 1998a,b). These elements include: Mo (Coveney et al., 1991; Dean et al., 1999); V–Ni relationships (Lewan and Maynard, 1982; Lewan, 1984; Breit and Wanty, 1991); U (Wignall and Meyers, 1988); Mn (Calvert and Pedersen, 1993); and rare earth elements or, more specifically, the Ce anomaly (Wright et al., 1987; Wilde et al., 1996; see German and Elderfield, 1990, for review). In addition, proxies for O_2 and HS^- (ΣH_2S) availability in ancient water columns have been developed based on degree-of-pyritization, which is a measure of the extent to which "reactive" iron has been transformed to pyrite (Berner, 1970; Raiswell et al., 1988); sulfur isotope trends (Muramoto et al., 1991; Calvert et al., 1996; Lyons, 1997); bacterial pigments indicative of anoxygenic photosynthesis in the presence of hydrogen sulfide (Repeta, 1993; Sinninghe Damsté et al., 1993); and pyrite framboid size distributions (Wilkin et al., 1996, 1997; Wignall and Newton, 1998). A number of studies of metal cycling in modern oxygen-deficient settings have helped refine these methods (Spencer and Brewer, 1971; Jacobs and Emerson, 1982; Jacobs et al., 1985; Anderson et al., 1989a,b; German and Elderfield, 1989; German et al., 1991; Lewis and Landing, 1992; Van Cappellen et al., 1998), including water-column work in the Cariaco Basin (Dorta and Rona, 1971; Bacon et al., 1980; Jacobs et al., 1987; de Baar et al., 1988) and detailed evaluations of Fe cycling (Lewis and Landing, 1991; Canfield et al., 1996; Lyons, 1997; Raiswell and Canfield, 1996, 1998; Hurtgen et al., 1999; Wijsman et al., 2001) and Mo cycling (Francois, 1988; Emerson and Huested, 1991; Colodner et al., 1995; Crusius et al., 1996; Helz et al., 1996; Dean et al., 1999; Zheng et al., 2000; Adelson et al., 2001).

The present study of Site 1002 of Leg 165 of the Ocean Drilling Program has a threefold geochemical agenda focused specifically on the temporal juxtaposition of oxic and anoxic deposits marking the last glacial–interglacial transition: (1) C_{org}–S_{py} relationships-including S isotope records, syngenetic (water-column formed) vs. diagenetic pyrite formation, and, in particular, the manifestation of diffusional overprinting by dissolved sulfide; (2) Fe/Al ratios and their implications with regard to the balance between

detrital Fe inputs and Fe scavenged in the sulfidic water column during pyrite formation; and (3) Mo/Al relationships as a possible record of water-column redox or, more specifically, of Mo deposition coupled to organic matter accumulation in the presence of hydrogen sulfide in the water column and pore fluids. The results of our study show that S_{py} and Fe relationships in the sediments are strongly influenced, through primary and secondary Fe sulfide mineralization, by the presence of hydrogen sulfide in the anoxic water column (compare Werne et al., 2003, this volume). The link between Mo enrichment in the sediments and euxinic conditions in the water column is less clear.

2. Regional setting

The 160 × 60-km Cariaco Basin on the northern continental shelf of Venezuela is the world's second-largest modern anoxic basin, following the Black Sea (Richards, 1975). The basin consists of two sub-basins with maximum water depths of about 1400 m separated by a central saddle, which shallows to approximately 900 m (Fig. 1). Exchange with the open Caribbean Sea is restricted by a series of low sills. The deepest present-day connections through these sills (~ 146 and ~ 120 m on the western and northern margins of the basin, respectively) provide a steady sub-thermocline source of nutrients, which stimulate production in the photic zone. The otherwise inhibited horizontal exchange, in combination with the organic-carbon loading and a strong pycnocline capable of limiting vertical exchange, results in anoxic–sulfidic conditions below approximately 300 m. These and other hydrographic, bathymetric, and geochemical details for the modern Cariaco Basin are provided in Richards and Vaccaro (1956), Richards (1975), Bacon et al. (1980), Jacobs et al. (1987), Scranton et al. (1987), de Baar et al. (1988), Fry et al. (1991), Peterson et al. (1991), and Muller-Karger et al. (2000).

The Cariaco Basin has been intermittently anoxic over at least the last ~ 580 ky, as recorded in C_{org} accumulation and concentrations (Haug et al., 1998; Peterson et al., 2000; Werne et al., 2000b), relative concentrations of redox-sensitive metals (V, Mn, Fe, and Mo; Dean et al., 1999; Yarincik et al., 2000a), the distribution of bioturbated vs. microlaminated sedi-

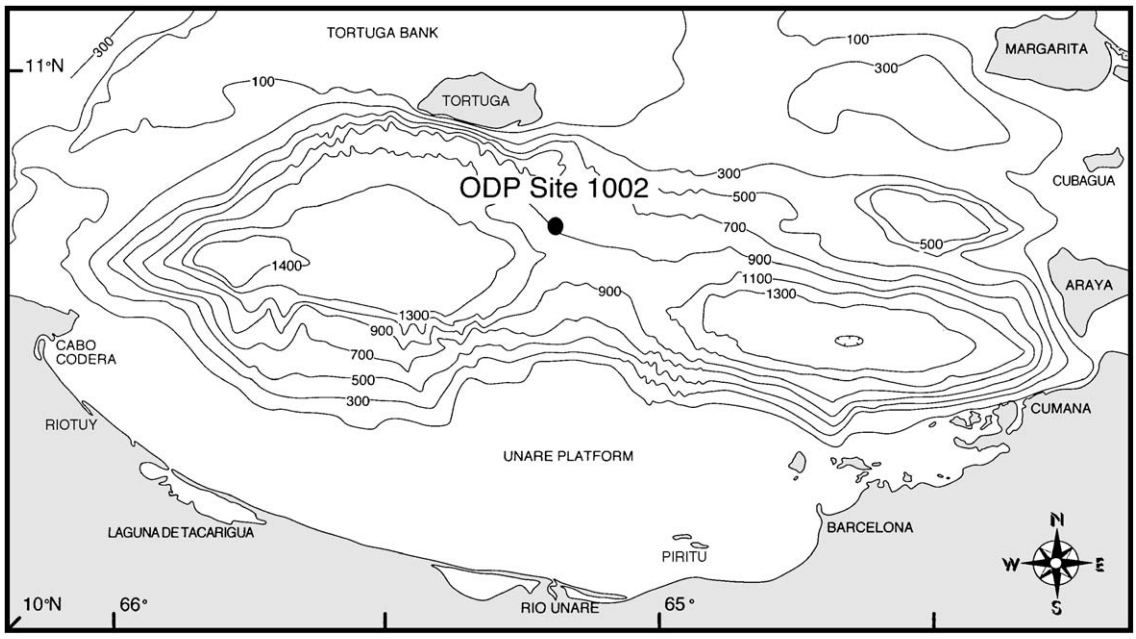

Fig. 1. Location and bathymetric map of the Cariaco Basin showing position of Site 1002 of Ocean Drilling Program (ODP) Leg 165 (February 1996).

ment (Peterson et al., 2000), and indirectly through nitrogen isotope records (Haug et al., 1998). Several recent studies have linked this temporal variation in water-column redox, and specifically the most recent transition from oxic to anoxic conditions, to glacioeustatic sea-level fluctuations recorded in the oxygen isotope records of planktonic foraminifera (Peterson et al., 1991, 2000; Lin et al., 1997; Haug et al., 1998; Yarincik et al., 2000a). Sea level controls the extent to which the basin receives only nutrient-depleted waters from the surface mixed layer of the Caribbean Sea vs. nutrient-rich waters from thermocline depths, which via their controls on primary production ultimately dictate respiratory oxygen consumption (Haug et al., 1998). Therefore, glacial–interglacial transitions are marked by a shift from oxic to anoxic conditions as sea level rose and nutrient-rich waters entered the basin.

Following the last glacial recession and concomitant rise in sea level, anoxia developed in the Cariaco Basin at ~ 12.6 ^{14}C ky before present (ka BP) or roughly 14.5 calendar ka BP (Peterson et al., 1991; Hughen et al., 1996a,b, 1998; Lin et al., 1997). At this transition, pronounced shifts in paleontological and paleoceanographic parameters independently constrain depositional oxygen levels and thus set the stage for the geochemical data interpreted in the present study. The foraminiferal assemblage, for example, is characterized by a disappearance of the benthic species across the transition from oxic to anoxic deposition and a corresponding shift from dominance by a warm-water planktonic taxon (*G. ruber*) to a fauna dominated by a subpolar species (*G. bulloides*) with an affinity for tropical upwelling environments (Peterson et al., 1991; Lin et al., 1997). This ecological transition is consistent with the introduction of cold, nutrient-rich waters linked to the rise in sea level.

Throughout this persistently anoxic interval over the last ~ 14.5 calendar ky, a strong seasonality in deposition is expressed in the microlaminated (varved) nature of the sediment (Hughen et al., 1996a). During the winter months, the Intertropical Convergence Zone (ITCZ) is located in its most southerly position (south of the equator), which drives strong trade winds above the Cariaco Basin and thus intense upwelling induced by Ekman transport. The corresponding microlamina within the seasonal couplet is comparatively thick and light-colored, reflecting high winter–spring productivity and a corresponding accumulation of opaline and, to a lesser extent, $CaCO_3$ tests (Hughen et al., 1996a). During the summer, the ITCZ moves north to a position more coincident with the basin, which weakens the trade winds and, correspondingly, the Ekman-induced upwelling (Peterson et al., 1991; Lin et al., 1997). The summer–fall microlamina is characterized by an abundance of darker siliciclastic material deposited during the local rainy season in combination with comparatively reduced productivity. Because of this well-preserved seasonal record and the high rates of sedimentation (30 to >100 cm/ky), the Cariaco is an ideal setting for high-resolution paleoceanographic studies (Peterson et al., 2000).

The model for seasonal variation in the Cariaco Basin has been extended to explain longer-term patterns in the region. Peterson et al. (1991) proposed that climatic patterns during the Younger Dryas cold period (YD; ~ 11.6 to 13.0 calendar ka BP; Hughen et al., 1998) were similar to those of present-day winter, resulting in generally stronger trade winds and therefore more intense upwelling relative to the depositional conditions of the over- and underlying microlaminated sediments. As a result, the YD was characterized by a diatom-rich planktonic ecosystem and overall greater productivity as seen in the thicker laminae and higher opal and C_{org} accumulation throughout this interval (Hughen et al., 1996a,b; Shipboard Scientific Party, 1997; Werne et al., 2000b). The generally stronger trade winds during the YD resulted in an increased flux of rutile-rich eolian material from the Sahara region and thus the lowest bulk Al/Ti ratios observed within the most recent anoxic interval (Yarincik et al., 2000b). Analogous temporal variations in Al/Ti ratios are recorded on glacial–interglacial time scales within the basin.

3. Core description and sampling protocol

The samples analyzed in the present study are from Site 1002 (February 1996) of Leg 165 of the Ocean Drilling Program (Fig. 1). The cores were collected by advanced hydraulic piston coring (APC) at a water depth of approximately 900 m, with recovered lengths of 9.77 and 6.24 m for cores 1002A and 1002B, respectively. Detailed sediment core locations and descriptions are available in Shipboard Scientific

Party (1997). Core 1002A overpenetrated by approximately 0.7 m below the seafloor, thus a mudline (sediment–water) interface was not collected. However, the redox transition at ~ 14.5 calendar ka BP—the focus of the present study—was retrieved successfully. By contrast, the mudline was recovered in core 1002B, but the core was of insufficient length to penetrate the redox transition. The geochemical records of the two cores were spliced together using the magnetic susceptibility records available in Shipboard Scientific Party (1997).

Cores 1002A and 1002B were collected for dedicated geochemical study. Subsamples of 5-cm thickness were used throughout the present study, although the intervals between the analyzed 5-cm samples were not the same for all the procedures. The whole-round 5-cm samples from core 1002B were processed for interstitial waters using a trace-metal noncontaminated titanium squeezer. (Pore-water data are not addressed in the present paper [see Werne et al., 2003, this volume, for pore-water sulfate and sulfide results]). The resulting "squeeze cakes" were frozen immediately for later analysis of the solid-phase constituents. Unsqueezed, 5-cm whole-round samples from core 1002A were immediately frozen for later analysis of the solids. Prior to analysis, frozen samples were dried oxically at ~ 40 °C and gently disaggregated using a ceramic mortar and pestle.

3.1. Stratigraphy and sedimentology

General stratigraphic and age relationships are summarized in Fig. 2, and highlights of published descriptive details are provided here as an essential context for the geochemical results. The sediments of the upper ~ 6.5 m below the seafloor (~ 14.5 calendar ka BP to present) at Site 1002 are dark olive gray, organic-rich silty clay with nannofossils and foraminifera grading downward into diatom-rich clayey mud with abundant calcareous microfossils (Subunit IA of Shipboard Scientific Party, 1997). These sediments are undisturbed by bioturbation and are thus weakly to distinctly laminated throughout the section. The laminae typically show thicknesses of millimeter to submillimeter scale and are thicker and more distinct where diatoms are abundant (Shipboard Scientific Party, 1997). A comparison between counts of paired laminae and independent ^{210}Pb chronologies suggest that the

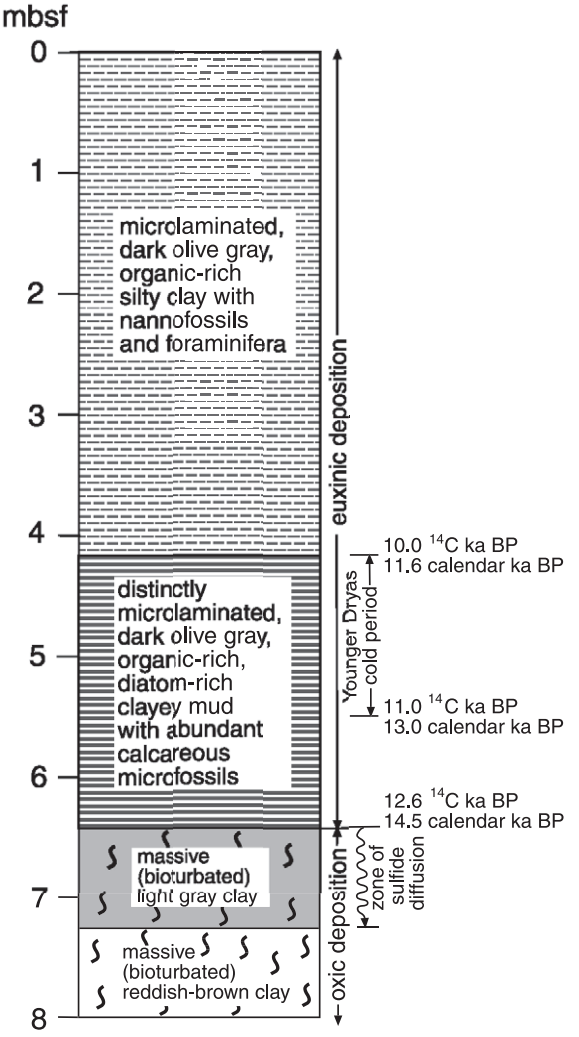

Fig. 2. Stratigraphic column with lithologic descriptions for Site 1002. Depths represent meters below the seafloor (mbsf). The abrupt shift from oxic to euxinic deposition during the most recent glacial–interglacial transition is delineated. Also shown are the Younger Dryas cold period—a time of high primary production in the basin—and the zone of sulfide diffusion, where oxically deposited, bioturbated sediments were overprinted by diffusing hydrogen sulfide following the shift from oxic to euxinic deposition. Age estimates for critical boundaries are included. Details for all these features are available in the text and in references cited therein.

light–dark sediment couplets record seasonal variation and are thus true varves (Hughen et al., 1996a).

Thin (centimeter-scale), homogeneous light gray clay layers within the microlaminated sediments are likely muddy microturbidites (Hughen et al., 1996a),

which are thinner but otherwise similar to those observed in the Black Sea (Lyons, 1991). These readily visible microturbidites constitute at most a few percent of the total microlaminated sediment record, although Hughen et al. (1996a) suggested that very thin (from 4 to <0.5 mm) microturbidites occur throughout the microlaminated sediment. Additional chronologic, sedimentologic, and paleoceanographic details are available for these varved sediments (Peterson et al., 1991; Hughen et al., 1996a,b, 1998; Lin et al., 1997; Shipboard Scientific Party, 1997).

The most obvious feature of the spliced (1002A–1002B) sediment record is the abrupt downward transition at ~6.5 mbsf (meters below the seafloor) from microlaminated deposits to the underlying massive (bioturbated) light gray clay. This massive gray clay grades downward at ~7.3 mbsf into massive reddish-brown clay; together, these massive clays constitute Subunit IB of Shipboard Scientific Party (1997). As with the transition between laminated and nonlaminated sediment above, the gray-to-red gradation in relatively sharp, being confined to a roughly 1- to 2-cm interval. The reddish-brown material extends downward to the base of the interval of interest (8.0 mbsf). On close inspection, the "massive" gray and reddish-brown material ranges from mottled to perhaps faintly (cm-scale) gray–black color banded. In contrast to the anoxic deposition indicated for the microlaminated sediment, the gray and reddish-brown clays show evidence for bioturbation and thus oxic conditions (Peterson et al., 1991; Lin et al., 1997; Shipboard Scientific Party, 1997).

4. Analytical methods

Concentrations of total and inorganic C in powdered samples were determined via combustion (950 °C) and acidification (~2 N HCl), respectively. The evolved CO_2 was quantified using a UIC carbon coulometer (Huffman, 1977), and total C_{org} was calculated by difference. Analytical errors of less than 1% were obtained for replicate analyses of a pure $CaCO_3$ standard and marine sediment samples.

Splits of the powdered dry samples were also analyzed for concentrations of total reduced inorganic sulfur (TRIS: pyrite S + acid-volatile sulfide S + elemental S) using the chromium reduction method (Canfield et al., 1986; Lyons and Berner, 1992). Wet, homogenized, previously frozen samples from the upper 50 cm of core 1002B were extracted for acid-volatile sulfide (AVS, "FeS") at room temperature using 6 N HCl containing 15% $SnCl_2$ (Berner et al., 1979; Chanton and Martens, 1985; Morse and Cornwell, 1987). Separate determinations of elemental sulfur (S°) were not performed. Sulfur yields of 96–98% are typical for freshly ground pyrite standards using chromium reduction. Replicate analyses of marine samples generally yield a reproducibility of ±2% or better. Recoveries averaging 98% are achieved for CdS standards using the HCl–$SnCl_2$ extraction. (Our past work has shown that AVS oxidizes during drying to a phase [likely S°] that is still extracted during chromium reduction).

All concentration data are reported on a dry-sediment basis. For the wet-sediment (AVS) extractions, a separate sample split was weighed wet and dry to determine water content. We did not correct the wt.% data for salt content, as the bulk dried solids (particularly the squeezed intervals) contain less than 5–10% salt. Also, elemental ratios are not affected by salt contents.

Sulfur isotope compositions of the bulk TRIS were measured on Ag_2S precipitates of the sulfide liberated during chromium reduction (Newton et al., 1995; Lyons, 1997). Aliquots of the Ag_2S were placed in tin boats with V_2O_5 catalyst and combusted online using a Carlo Erba elemental analyzer connected via continuous gas flow to a Finnigan 252 isotope ratio monitoring mass spectrometer at Indiana University, Bloomington. Sulfur isotope compositions are expressed as permil (‰) deviations from V-CDT using the conventional delta notation. Sulfur isotope results are generally reproducible within ±0.1‰.

Degree-of-pyritization (DOP) measurements provide an estimate of the Fe remaining for reaction with dissolved sulfide (Berner, 1970; Raiswell et al., 1988). More specifically, DOP is an approximation of the extent to which the original total "reactive" Fe has been transformed to pyrite and can be expressed as:

$$\mathrm{DOP} = \frac{(\text{pyrite Fe})}{(\text{pyrite Fe}) + (\text{extractable Fe})},$$

where "extractable Fe" is traditionally defined as the remaining unsulfidized portion of the Fe pool having

the potential to react with HS^-. In this and many other studies, this "reactive" Fe is operationally defined as the fraction of total solid-phase Fe readily dissolved during a 1 min, boiling 12 N HCl distillation (see Lyons and Berner, 1992; Lyons, 1997). Traditional arguments state that DOP values track depositional redox, with values of ~0.75 or greater suggesting anoxic to anoxic–sulfidic deposition, while lower values are more consistent with a weakly to strongly oxic water column (Raiswell et al., 1988). Recent work has demonstrated, however, that the boiling HCl approach may overestimate the readily reactive Fe by including Fe-bearing phases that require prolonged exposure to HS^- for transformation to iron sulfides ($\geq 10^2$ years, much greater in many cases) and that the paleoredox model of Raiswell et al. (1988) may be an oversimplification (Canfield et al., 1992, 1996; Raiswell et al., 1994, 2001; Raiswell and Canfield, 1996, 1998; Lyons, 2000). Nevertheless, the traditional DOP approach can yield unambiguous paleoenvironmental information.

Metal concentrations in bulk dried powders were determined by $HF/HNO_3/HClO_4$ digestion and quantification via inductively coupled plasma emission spectrometry (ICP-ES). Reproducibility was generally better than 5% for Mo solid concentrations in the range of 10^1–10^2 ppm. Concentrations of Mo in the 10^0–10^1 ppm range were reproducible within 10% to 20%. Replicate Fe and Al analyses generally agreed within a few percent. Data for Fe and Mo are normalized to Al rather than Ti because of the temporal variation in Ti input; we are assuming that the ratios of Fe and Mo to Al for the continental inputs have not varied over the time interval of interest.

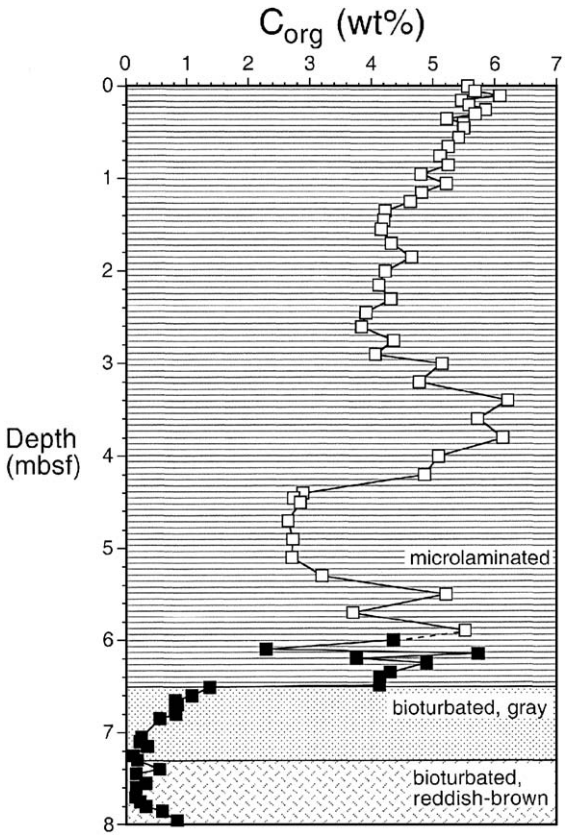

Fig. 3. Depth profile of total organic carbon (C_{org}) concentrations for both oxic and euxinic sediments spanning the most recent glacial–interglacial transition in the Cariaco Basin (ODP Site 1002). Sediment depths are expressed as meters below the seafloor (mbsf). The open squares represent 5-cm intervals from core 1002B; the closed squares represent 5-cm intervals from core 1002A. Important lithologic and geochemical units are also shown. See Fig. 1 and text for details.

5. Results

5.1. Carbon and sulfur concentrations

Concentrations of C_{org} decrease monotonically over the upper ~3.0 mbsf from a surface value of ~6.0 wt.% to a value of ~4.0 wt.% (Fig. 3 and Table 1). A subsurface maximum occurs between roughly 3.0 and 4.0 mbsf followed by a broad minimum spanning from ~4.0 to 5.5 mbsf, where C_{org} values drop below 3.0 wt.%. Below this minimum, the data scatter around a mean C_{org} concentration of about 4.5 to 5.0 wt.%, followed by a sharp downcore decrease at 6.5 mbsf. This decrease is coincident with the transition from microlaminated to gray, bioturbated sediment. Concentrations of C_{org} drop systematically over the upper 50 cm of the gray clay from a value of ~1.5 wt.% to values <0.5 wt.%. With the exception of a subtle increase in the basal 20 cm of the studied interval (Fig. 3), C_{org} concentrations remain uniformly low across the gray–red transition and into the reddish-brown clay.

In the microlaminated interval, concentrations of AVS are consistently below 0.05 wt.% in the upper 50 cm, which is approaching the lower limit of detection

Table 1
Geochemical data

Depth (cm below seafloor)	Total inorganic carbon (wt.%)	Total organic carbon (C_{org}) (wt.%)	Pyrite sulfur (S_{py}) (wt.%)[a]	S_{py} carbonate-free basis (wt.%)[a]	$\delta^{34}S_{py}$ (‰)[a]	Total iron (Fe_T) (wt.%)	Total aluminum (wt.%)	Fe_T/Al	HCl-soluble iron (Fe_{HCl}) (wt.%)	Degree-of-pyritization (DOP)	Dithionite soluble iron (Fe_D) (wt.%)	Total molybdenum (ppm)	Mo/Al
0	3.84	5.56	1.31	1.93					1.16	0.50			
5	3.78	5.68	1.28	1.87	− 32.6				1.04	0.52			
10	3.71	6.08	1.15	1.66	− 33.2	2.78	5.86	0.48	1.07	0.48		95	0.00163
15	3.87	5.46	1.27	1.87	− 31.9	2.73	6.15	0.44	1.00	0.53	0.21	80	0.00130
20	3.86	5.58	1.34	1.98	− 33.8				1.06	0.52			
25	3.85	5.85	1.23	1.81	− 33.3	2.70	5.80	0.47	0.97	0.53		93	0.00160
30	3.99	5.68	1.63	2.44	− 32.7	2.82	5.58	0.50	1.09	0.57		112	0.00201
35	3.92	5.22	1.39	2.06	− 32.9				1.03	0.54	0.20		
40	4.03	5.49	1.22	1.84	− 32.7				1.12	0.49			
45	3.78	5.50	1.22	1.78		2.89	6.03	0.48	0.94	0.53		103	0.00171
55	4.27	5.42	1.38	2.14	− 32.3	2.83	5.80	0.49	0.98	0.55	0.13	97	0.00167
65	4.00	5.25	1.39	2.08					0.93	0.57	0.14		
75	3.92	5.12	1.50	2.23	− 32.9				1.06	0.55			
85	3.66	5.25	1.29	1.86		3.07	6.13	0.50	0.96	0.54		97	0.00158
95	4.17	4.81	1.60	2.45	− 31.3				1.07	0.57			
105	3.94	5.22	1.43	2.13	− 31.7				0.96	0.57			
115	3.62	4.82	1.46	2.09		3.16	6.28	0.50	1.12	0.53		78	0.00124
125	4.20	4.64	1.43	2.20	− 33.2	2.77	5.53	0.50	0.89	0.58	0.13	82	0.00148
135	3.85	4.23	1.63	2.40					1.05	0.58			
145	4.34	4.21	1.41	2.21	− 33.8				0.97	0.56	0.10		
155	3.86	4.17	1.58	2.33		3.15	6.16	0.51	1.04	0.57		47	0.00076
170	3.93	4.33	1.64	2.44	− 32.8				1.03	0.58	0.12		
185	3.55	4.66	1.58	2.24					1.10	0.56			
200	3.56	4.23	1.59	2.26					1.08	0.56			
215	3.77	4.13	1.51	2.20		3.13	6.38	0.49	1.05	0.56	0.14	79	0.00124
230	3.64	4.32	1.45	2.08	− 33.8				1.03	0.55			
245	3.74	3.92	1.57	2.28					1.06	0.56			
260	3.83	3.85	1.64	2.41		3.24	6.40	0.51	1.06	0.57		81	0.00127
275	3.69	4.37	1.60	2.31	− 17.5				1.01	0.58	0.18		
290	3.61	4.07	1.51	2.16		3.37	6.56	0.52	1.13	0.54	0.14	95	0.00145
300	3.42	5.15	1.55	2.17	− 30.5				1.09	0.55			
320	3.17	4.78	1.53	2.08					1.11	0.55	0.18		
340	2.96	6.21	1.56	2.07		3.40	6.61	0.51	1.10	0.55		163	0.00247
360	3.17	5.72	1.55	2.11					1.11	0.55	0.15		
380	2.94	6.13	1.43	1.89	− 27.8	3.10	5.94	0.52	1.00	0.56		187	0.00315
400	3.03	5.09	1.18	1.58					0.90	0.53			
420	3.31	4.86	1.21	1.67					0.77	0.58			

440	3.94	2.89	0.92	1.37		1.97	3.90	0.51	0.63	0.56		67	0.00172
445	3.91	2.74	0.98	1.46	− 27.4				0.69	0.55	0.14		
450	3.52	2.85	0.93	1.32	− 26.2	1.91	3.78	0.51	0.66	0.55		62	0.00164
470	3.82	2.65	1.00	1.46		2.04	3.89	0.53	0.69	0.56	0.11	60	0.00154
490	3.76	2.73	1.18	1.72		2.35	4.46	0.53	0.80	0.56		64	0.00144
510	4.02	2.71	1.17	1.76	− 28.2	2.56	5.01	0.51	0.90	0.53	0.13	65	0.00130
530	3.59	3.20	1.22	1.74		2.83	5.54	0.51	0.97	0.52	0.16	103	0.00185
550	3.08	5.21	1.22	1.64		2.62	4.85	0.54	0.77	0.58		154	0.00318
570	2.19	3.70	1.93	2.36		3.24	6.05	0.54	0.96	0.64		146	0.00241
590	2.63	5.51	1.68	2.15	− 26.5	2.82	5.10	0.55	0.65	0.69		178	0.00349
600	2.53	4.35	1.65	2.09	− 28.4	3.63	7.15	0.51				180	0.00252
610	1.05	2.29	2.29	2.51	− 25.5	4.33	8.50	0.51				144	0.00169
615	1.04	5.72	1.61	1.76	− 26.1								
620	1.56	3.75	1.94	2.23	− 27.4	3.50	6.85	0.51				162	0.00236
625	2.84	4.89	1.82	2.38	− 28.3								
635	2.21	4.30	2.01	2.46		3.90	7.65	0.51				172	0.00225
640	2.27	4.13	2.10	2.59									
648.75[b]	2.31	4.13	2.31	2.86	− 27.9	3.93	7.42	0.53				162	0.00218
651.25[c]	0.75	1.37	3.04	3.24	− 28.7	4.87	9.55	0.51				76	0.00080
660	2.85	1.08	1.96	2.57	− 30.5	3.65	7.66	0.48				8	0.00010
665	3.05	0.81	1.91	2.56	− 29.1								
670	2.73	0.84	1.82	2.36	− 27.4	3.70	8.27	0.45				3	0.00004
675	2.60	0.81	1.89	2.41	− 24.5								
680	3.42	0.82	1.82	2.55	− 23.0								
685	2.21	0.56	2.12	2.60		3.95	8.45	0.47				3	0.00004
705	0.79	0.26	2.75	2.94	− 12.2								
710	0.60	0.23	2.65	2.79	− 12.8	4.70	9.79	0.48				5	0.00005
715	1.10	0.36	2.77	3.05	− 13.0								
725	0.14	0.13	2.47	2.50	− 8.8	4.90	9.79	0.50				3	0.00003
730[d]	0.32	0.19	0.50	0.52	− 7.8	4.82	11.10	0.43				3	0.00003
740	0.50	0.55	0.12	0.12	− 27.2	4.98	11.10	0.45				2	0.00002
745	0.28	0.17	0.11	0.11	− 13.4								
755	0.68	0.33	0.18	0.19									
760	0.30	0.17	0.06	0.06	− 23.0	5.18	10.90	0.48				2	0.00002
770	0.20	0.16		0.00	+16.7								
775	0.59	0.23	0.17	0.18	+3.9								
780	1.05	0.33	0.27	0.29	+19.1								
785	1.77	0.59	0.41	0.48	− 8.3	4.16	9.06	0.46				2	0.00002
795	2.34	0.83	0.57	0.71	− 21.6								

[a] S_{py} data represent TRIS as determined by chromium reduction of bulk dry sediment. In the present study, TRIS is assumed to consist entirely of S_{py}. See text for details.
[b] Base of microlaminated interval.
[c] Top of gray interval—note that samples at the interface contain minor amounts of sediment from the adjacent interval.
[d] Transition between gray and red intervals.

for our AVS method. No suggestion of AVS enrichment existed deeper in the core other than some gray–black mottles and banding best expressed within the reddish-brown clay. These colorations may represent localized sites of enhanced sulfate reduction. In a complementary study (Werne et al., 2003, this volume), chromium reduction extractions of untreated, bulk-sediment samples and bitumen-extracted residues showed insignificant differences in sulfur yields, confirming that the chromium reduction method is not extracting bitumen sulfur. Given these observations and the expectation that S° concentrations are low relative to iron sulfide in this highly reducing setting, the total Cr-reducible S (TRIS) is assumed to represent S_{py}.

Concentrations of S_{py} show a subtle downcore increase over the upper 3.8 m, with a mean value of 1.45 ± 0.14 wt.% ($\pm 1\sigma$, $n = 35$) (Fig. 4 and Table 1). Between approximately 4.0 and 5.5 mbsf, S_{py} concentrations decrease to values ranging from ~0.9 to 1.2 wt.% before increasing to 1.93 wt.% at 5.7 mbsf. Over the remaining, basal portion of the microlaminated sediment, S_{py} concentrations range between ~1.6 and 2.3 wt.% before increasing sharply to 3.04 wt.% in the uppermost bioturbated gray clay at the interface with the overlying microlaminated sediment. The gray clay below the interface enrichment has S_{py} concentrations ranging between ~1.8 and 2.8 wt.%, with a mean of 2.22 ± 0.40 wt.% ($n = 10$). At the transition between the gray and reddish-brown clay, the S_{py} concentration drops abruptly to 0.50 wt.% and stays low throughout the underlying interval (mean: 0.23 ± 0.18 wt.%, $n = 8$), while covarying positively with the concentrations of C_{org} ($r^2 = 0.72$; plot not shown).

Pyrite sulfur concentrations are summarized on a carbonate-free basis in Fig. 5 and Table 1 to address possible dilution effects associated with biogenic $CaCO_3$ (see also Werne et al., 2000b, 2003, this volume). Inorganic ($CaCO_3$) carbon concentrations are available in Table 1. With the exception of the basal portion of the interval, calculated $CaCO_3$ concentrations within the microlaminated sediment fall between approximately 25 and 35 wt.%. In the basal portion of the laminated zone and throughout the underlying gray and reddish-brown clay, $CaCO_3$ contents are lower and significantly more variable than in the overlying microlaminated sediments. Although the

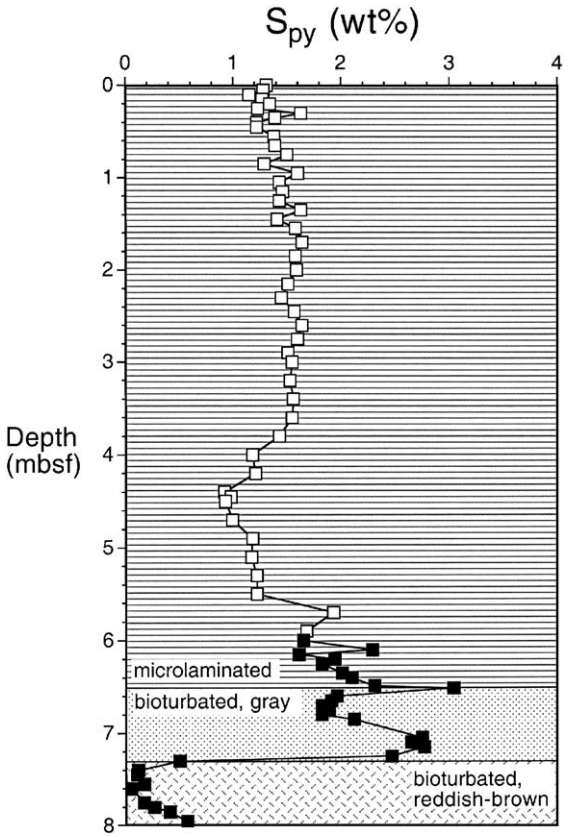

Fig. 4. Depth profile of pyrite sulfur (S_{py}) concentrations for both oxic and euxinic sediments spanning the most recent glacial–interglacial transition in the Cariaco Basin (ODP Site 1002). Data represent total inorganic reduced sulfur (TRIS) as determined by the chromium reduction method. In the present study, TRIS is assumed to consist entirely of S_{py}. The open squares represent 5-cm intervals from core 1002B; the closed squares represent 5-cm intervals from core 1002A.

$CaCO_3$ content is variable and the S_{py} data are shifted toward higher values when expressed on a carbonate-free basis, the general shapes of carbonate-free and whole-sediment S_{py} plots are very similar (compare Figs. 4 and 5).

5.2. Sulfur isotope ratios

Sulfur isotope data for pyrite are presented in Fig. 6 and Table 1. With the exception of the one outlier at 2.8 mbsf (-17.5‰), the $\delta^{34}S$ data in the upper ~3.0 mbsf are within 1‰ to 2‰ of the present-day bottom-water dissolved sulfide value (-31‰ to

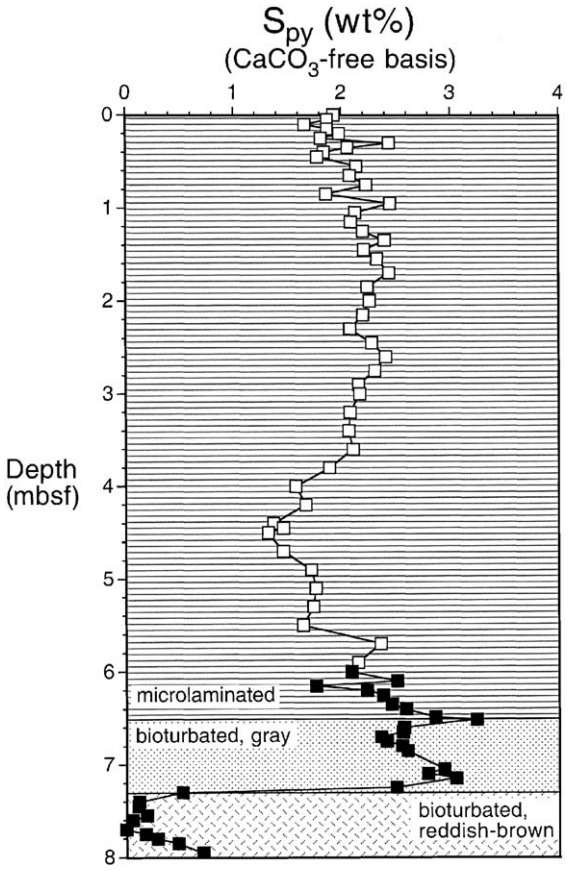

Fig. 5. Depth profile of S_{py} concentrations presented on a $CaCO_3$-free basis (to assess carbonate dilution effects) for both oxic and euxinic sediments spanning the most recent glacial–interglacial transition in the Cariaco Basin (compare Fig. 4). The open squares represent 5-cm intervals from core 1002B; the closed squares represent 5-cm intervals from core 1002A.

$-32‰$; Fry et al., 1991). The mean for these data (excluding the outlier) is $-32.7 \pm 0.9‰$ ($n=17$). Below 3.0 mbsf, the data for the microlaminated sediments show a subtle downcore shift toward ^{34}S enrichment, reaching a maximum value of $-25.5‰$ at 6.1 mbsf (see also Werne et al., 2003, this volume). Within the gray clay, $\delta^{34}S$ values increase uniformly downcore from a minimum value of $-30.5‰$ just below the contact with the microlaminated sediment to a maximum of $-7.8‰$ at the transition between gray and reddish-brown clay. Within the reddish-brown clay, the $\delta^{34}S$ values are highly scattered and range between $-27.2‰$ and $+19.1‰$.

5.3. Iron

Iron concentrations within the Cariaco sediments are presented using a fourfold speciation scheme: total Fe (Fe_T), pyrite Fe (Fe_{py}), acid-soluble Fe (Fe_{HCl}), and iron extracted by dithionite (Fe_D). Concentrations of Fe_T and total Al are summarized in Table 1 and

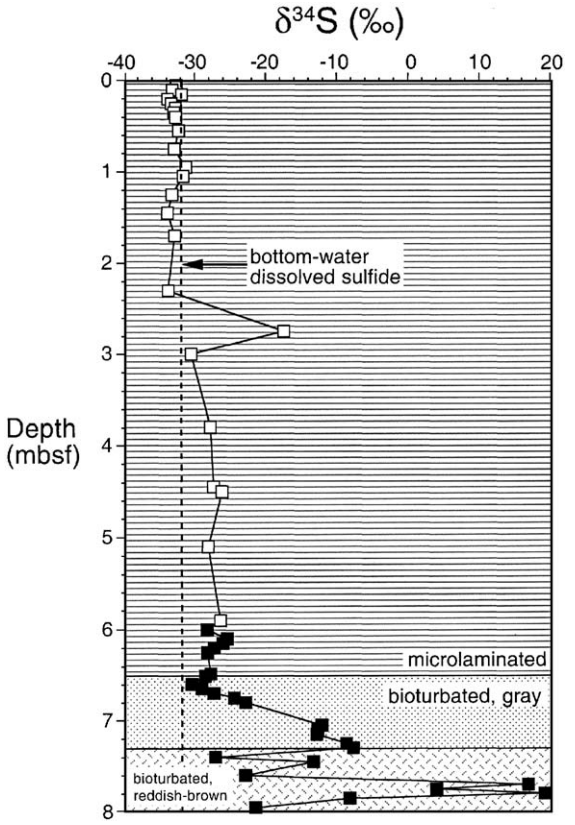

Fig. 6. Depth profile of the isotope composition of S_{py} for both oxic and euxinic sediments spanning the most recent glacial–interglacial transition in the Cariaco Basin (ODP Site 1002). $\delta^{34}S$ values represent TRIS as determined by the chromium reduction method. The open squares represent 5-cm intervals from core 1002B; the closed squares represent 5-cm intervals from core 1002A. A mean $\delta^{34}S$ value for modern dissolved water-column sulfide (Fry et al., 1991) is also provided. Note that the Fry et al. data are reported relative to CDT but also that the difference between CDT and V-CDT is, for our purposes, negligible ($<1‰$; Ding et al., 2001). Also, Fry et al. show little S isotope variability with depth and provide no detailed data for the chemocline region, thus it is not possible to use S isotopes to delineate the specific depth of pyrite formation in the water column (compare Muramoto et al., 1991; Lyons, 1997).

presented as Fe_T/Al ratios in Fig. 7 and Table 1. Fe_T concentrations range between roughly 2.0 and 5.0 wt.% with considerable scatter. Fe_T/Al ratios, which eliminate the effects of opal and calcium carbonate dilution and allow us to address enrichments or depletions relative to an average detrital (continental) input, are lowest in the surface interval and within the gray and reddish-brown clay at the base of the section, reaching minima of 0.43–0.44. A subtle downcore increase in Fe_T/Al ratios, with scatter, occurs over the upper 100 cm. The ratios are generally above 0.50 throughout the remainder of the microlaminated sediment—reaching values as high as 0.55. Within the gray and reddish-brown clay interval, Fe_T/Al values are variable and, with one exception, well below 0.50.

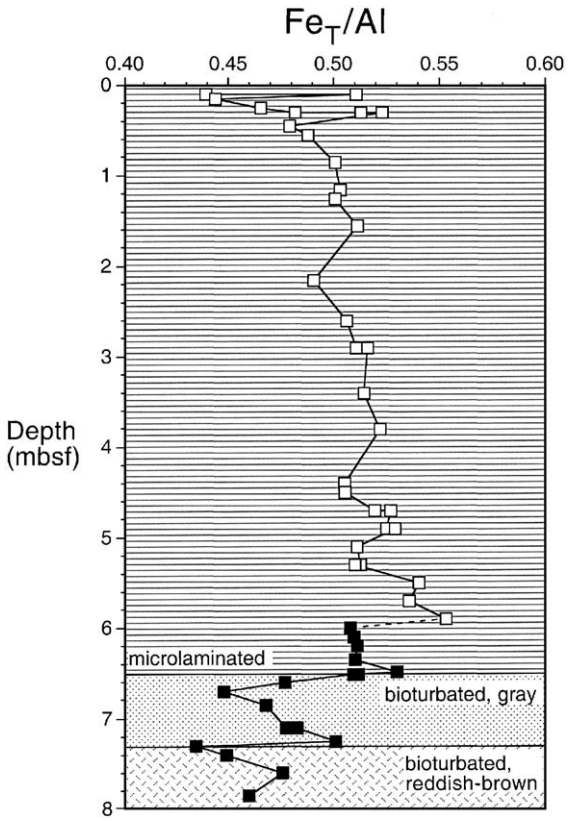

Fig. 7. Depth profile of total Fe (Fe_T) to Al ratios for both oxic and euxinic sediments spanning the most recent glacial–interglacial transition in the Cariaco Basin (ODP Site 1002). The open squares represent 5-cm intervals from core 1002B; the closed squares represent 5-cm intervals from core 1002A.

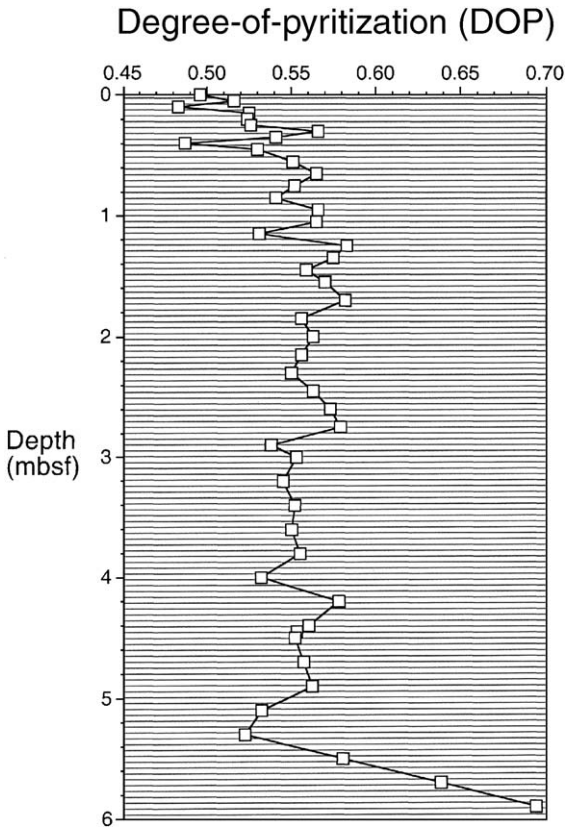

Fig. 8. Depth profile of degree-of-pyritization (DOP) values for the upper 5.9 m (core 1002B) of the uppermost euxinic interval in the Cariaco Basin.

Concentrations of Fe_{py} were calculated from TRIS data (Table 1) by assuming that TRIS is equivalent to S_{py}. Fe_{HCl} data are available for the upper 5.9 m of the microlaminated interval and are presented in Table 1. The Fe phases dissolved during this boiling HCl procedure are effectively summarized in Raiswell et al. (1994). DOP values calculated from Fe_{py} and Fe_{HCl} concentrations for the upper 5.9 m range between 0.48 and 0.69, with a mean of 0.55 ± 0.03 ($n = 47$). The DOP data show scatter but overall increase downcore from values between 0.48 and 0.50 in the upper 15 cm to 0.58 by 1.25 mbsf (Fig. 8 and Table 1), thereafter remaining relatively uniform before increasing abruptly and monotonically from 0.52 to 0.69 in the interval from 5.3 to 5.9 mbsf.

Fe_D represents iron soluble in a buffered (pH = 4.8) citrate-dithionite solution (Canfield, 1989; Raiswell et

al., 1994; Raiswell and Canfield, 1996, 1998). The dithionite approach has been shown to quantitatively extract iron oxides and oxyhydroxides (ferrihydrite, lepidocrocite, goethite, and hematite), with only small contributions from iron silicates (Canfield, 1989; Raiswell et al., 1994). Thus, Fe_D is dominantly a highly reactive iron fraction with respect to dissolved sulfide (Canfield et al., 1992). A limited number of Fe_D results and the methodological details are available for samples from the present study (upper 5.3 m) through the independent investigation of Raiswell and Canfield (1998) (mean: 0.15 ± 0.03 wt.%, $n = 16$; Table 1).

5.4. Molybdenum

Within the microlaminated zone, Mo concentrations are variable but uniformly high in the ~ 50–200 ppm range. Overall, however, concentrations of Mo show pronounced downcore variation (Table 1). The uppermost gray clay sample, which may include some of the overlying microlaminated material, contains 76 ppm relative to 162 ppm in the basal microlaminated sample; values less than 10 ppm occur throughout the remainder of the gray and reddish-brown clay.

The data expressed as Mo/Al ratios (Fig. 9 and Table 1), to remove dilution effects, also show

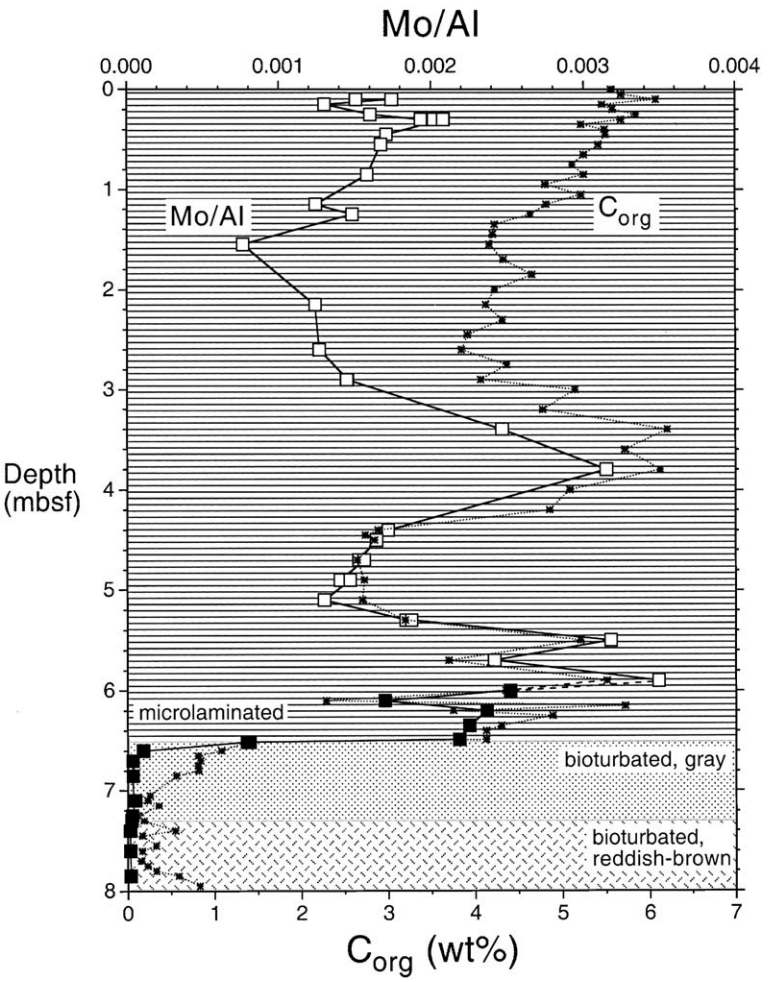

Fig. 9. Depth profile for total Mo to Al ratios for both oxic and euxinic sediments spanning the most recent glacial–interglacial transition in the Cariaco Basin (ODP Site 1002). Corresponding data for C_{org} concentrations are provided for comparison. The open squares represent 5-cm intervals from core 1002B; the closed squares represent 5-cm intervals from core 1002A.

comparatively high values throughout the microlaminated zone, generally falling between 0.001 and 0.003. Ratios of Mo/Al maintain low values in the range of 10^{-5} throughout the gray/reddish-brown interval. Organic-carbon variations are *generally* coherent with the downcore Mo/Al trend (Fig. 9), although the actual calculated correlation between the two parameters within the microlaminated interval is weak ($r^2 = 0.12$). Concentrations of C_{org} and the Mo/Al ratios in the gray/reddish-brown clay are both low relative to the overlying microlaminated sediments. There are no simple relationships between the Mo/Al and C_{org} data for the oxic sediments (Fig. 9). However, the Mo/Al ratios are approximately a factor of two higher in the gray (sulfide overprinted) sediment relative to the underlying reddish-brown clay.

6. Discussion

6.1. Pyrite formation

The specifics of pyrite formation in the uppermost microlaminated interval in the Cariaco are the subject of a companion paper (Werne et al., 2003, this volume) and will be addressed only briefly here in the context of alternative hypotheses. The S_{py} and DOP relationships (Figs. 4 and 8) could record a progressive ~10% increase in Fe sulfidation during diagenetic pyrite formation over the upper ~1.0 mbsf, which augments a largely fixed syngenetic reservoir (expressed in the surface layers). If so, the dip in S_{py} concentration between ~4.0 and 5.5 mbsf might reflect dilution by biogenic opal and $CaCO_3$ during the high productivity of the Younger Dryas cold period (Werne et al., 2000b). (The similarities between Figs. 4 and 5 suggest, however, that carbonate dilution is not a dominant control on the pattern of S_{py} distribution in the sediments.) This comparatively low amount of diagenetic pyrite formation is consistent with the $\delta^{34}S_{py}$ trend spanning the length of the microlaminated interval, which does not deviate significantly from the isotopic composition of present-day dissolved sulfide in the water column (Fig. 6). Syngenetic iron sulfide formation is also indicated by calculations suggesting that water-column Fe concentrations are controlled by equilibrium with greigite (Jacobs et al., 1987). The paucity of greigite and other "monosulfide" phases in the sediments and the S isotope relationships argue for rapid (water-column) transformation to pyrite. Similarly, the downcore decrease in C_{org} concentration could also reflect a steady-state scenario: progressive anaerobic remineralization during sulfate reduction, with additional diagenetic pyrite formation being limited by the availability of readily reactive Fe. Inconsistent with this simple steady-state model, however, Werne et al. (2000b) showed that accumulation-rate trends for C_{org} differ from the concentration relationships and accumulation rates expected under steady-state conditions. Furthermore, Fe_T/Al ratios (Fig. 7) vary over the microlaminated interval rather than remaining fixed, as would be predicted for a constant syngenetic pyrite flux with progressive diagenetic sulfidation of a uniform detrital Fe flux.

Given the nonsteady-state history of deposition (i.e., time-varying inputs of $CaCO_3$, opal, C_{org}, and siliciclastic sediment), Werne et al. (2003, this volume) adopted an accumulation-rate approach to pyrite formation (mass area^{-1} time^{-1})—further constrained by a detailed S isotope mass balance—rather than interpreting concentration trends. Werne et al. also suggested that the syngenetic pyrite flux might have varied over the last ~14.5 calendar ky as a function of the variable C_{org} production (Werne et al., 2000b), which resulted in temporally varying hydrogen sulfide production in the water column. Overall, the accumulation-rate approach yielded a larger fraction of diagenetic pyrite and a decidedly less systematic accumulation of diagenetic pyrite relative to that suggested by the steady-state model outlined above.

Despite the presence of high concentrations of pore-water sulfide (up to ~8 mM; Werne et al., 2003, this volume), Fe_D persists over the length of the microlaminated interval at low but uniform concentrations (Table 1). This persistence is consistent with the suggestion of Raiswell and Canfield (1998) and Wilkin and Arthur (2001) that some fraction of dithionite extractable Fe, which is conventionally viewed as "highly" reactive, does not react even after prolonged exposure to sulfide. The high concentrations of dissolved sulfide in the microlaminated sediments confirm the Fe-limited pyrite formation suggested by the downcore trends for S_{py} concentrations. As outlined below, intermediate (and largely

uniform) DOP values can result despite the abundance of HS^-, because the boiling HCl extraction yields an overestimation of the readily reactive Fe (see Section 6.3.1). Thus, the sediments are Fe-limited over the diagenetic time scales of observation (10^3 years), and only through substantially longer exposure to sulfide might the DOP values increase (and perhaps by only small amounts) through additional diagenetic pyrite formation (Raiswell and Canfield, 1996).

Pyrite formation in the reddish brown, bioturbated sediments is C_{org}-limited as indicated by the abundance of residual iron oxide present as red–brown pigments, the comparatively low S_{py} concentrations, and the strong covariance between concentrations of S_{py} and C_{org}. The overlying gray, bioturbated clay, on the other hand, shows significantly higher S_{py} concentrations despite similarly low levels of C_{org}, suggesting possible iron limitation and undoubtedly pyrite formation through diffusion of HS^- from the overlying euxinic sediments and water column.

6.2. Sulfide diffusion

The abrupt juxtaposition of sediments with very different chemical properties at the transition from oxic to anoxic deposition at ~6.5 mbsf (~14.5 calendar ka BP) led to a pronounced diffusional sulfur (pyrite) overprinting of the uppermost layers of the underlying, oxically deposited sediments of the last glacial episode (Fig. 4). Because of Fe limitation, which is common in euxinic settings (e.g., Raiswell and Berner, 1985; Calvert and Karlin, 1991; Lyons and Berner, 1992; Canfield et al., 1996; Lyons, 1997; Raiswell and Canfield, 1998; Wilkin and Arthur, 2001), excess HS^- diffused out of the water column and C_{org}-rich sediments into the underlying oxic layer and reacted with Fe phases originally preserved because of the low levels of C_{org}. This diffusion resulted in a pyrite overprint in the C_{org}-limited sediment. The diffusion front advanced to progressively greater depths as Fe was consumed, such that the rate and extent of advance reflected the balance between the amount of sulfide and the quantity and reactivity of the Fe. The downward transition from gray to reddish-brown sediment marks the lower limit of diffusion. The fact that downward diffusion of dissolved sulfide dominated over upward diffusion of dissolved iron from the bioturbated layers reflects the high abundance of sulfide in the euxinic interval relative to dissolved Fe production in the oxically deposited sediments (Raiswell et al., 1993; Raiswell, 1997).

The $\delta^{34}S_{py}$ values of the overprinted pyrite most proximal to the oxic–anoxic transition approximate the sulfur isotope composition of the HS^- in the modern euxinic water column. As the sulfide front advanced downward, the sulfide source evolved (in the restricted pore-water reservoir of the basal microlaminated sediments) such that $\delta^{34}S_{py}$ values became progressively higher. This progressive ^{34}S enrichment is recorded in the downcore increase in $\delta^{34}S_{py}$ values observed in the gray clay (Fig. 6). Analogous pyrite overprints have been observed beneath sapropels in the Mediterranean, where HS^- production within the organic-rich sediment out-competes the Fe supply and thus reacts within the comparatively Fe-rich but C_{org}-deficient underlying sediments (Passier et al., 1996, 1997).

In settings such as the Black Sea and Kau Bay, Indonesia—and in contrast to the persistently marine conditions indicated for the Cariaco Basin—the last glacial–interglacial transition is marked by a shift from freshwater to marine conditions as sea level rose to the elevation of sills that restricted marine inputs during glacial lowstands (Middelburg, 1991; Middelburg et al., 1991; Arthur and Dean, 1998). In simple terms, the transition is marked by an overprint of S_{py} on the freshwater deposits this overprint resulted from diffusion of seawater sulfate into the sulfate-limited underlying sediments, which contained sufficient C_{org} (or CH_4; Jørgensen et al., 2001) to support sulfate reduction at rates equal to or greater than the rate of replenishment by sulfate diffusion (Zaback et al., 1993) and an adequate reactive Fe supply to retain the HS^- as pyrite (Middelburg, 1991; Middelburg et al., 1991). Isotopically, the sulfur in the freshwater deposits is strongly enriched in ^{34}S, with $\delta^{34}S_{py}$ values falling close to those of the seawater sulfate (Middelburg, 1991; Middelburg et al., 1991). An analogous freshwater overprint has been reported in the Baltic Sea (Sternbeck and Sohlenius, 1997). These high $\delta^{34}S_{py}$ values approximating the seawater sulfate value confirm that diffusion of sulfate rather than sulfide dominated and that Fe and C_{org} (or CH_4) concentrations of the underlying sediments were sufficient to result in essentially closed-system pyrite

formation. An important implication of diffusion of dominantly water-column sulfate rather than sulfide into the freshwater deposits is that the Black Sea and similar silled basins (e.g., Kau Bay, Indonesia) must have evolved from (1) sulfate-limited freshwater conditions to (2) an *oxic* brackish/marine setting with comparatively low C_{org} accumulation to (3) the Fe-limited, euxinic marine pyrite formation observed today (see also Calvert and Karlin, 1991; Lyons and Berner, 1992; Calvert et al., 1996; Lyons, 1997; Wilkin and Arthur, 2001). Such a transition is consistent with recent, independent interpretations of the glacial–interglacial evolution of the Black Sea (Arthur and Dean, 1998). Comparative details of the two diffusional scenarios (i.e., sulfate vs. sulfide) are outlined in Table 2.

Scatter in the Fe_T/Al ratios of the oxic gray and reddish-brown clays in the Cariaco Basin may reflect Fe remobilization and its interrelationship with the simultaneously diffusing HS^-. Overall, however, the Fe_T/Al ratios approximate continental (detrital) inputs, as would be expected in the absence of syngenetic pyrite formation.

6.3. Controls on iron distribution

6.3.1. The model

The extent to which iron reacts with HS^- to form pyrite (i.e., the DOP value) has been used as a measure of bottom-water oxygenation (Raiswell et al., 1988). The simple argument asserts that the typically prolonged exposure of iron to the ubiquitous sulfide within euxinic basins (in the water column, at the sediment–water interface, and within the sediment) results in the reaction of a high percentage of the detritally delivered "reactive" iron with dissolved sulfide—i.e., high DOP values. In recent years, however, duration of sulfide exposure as the critical control has been questioned. These challenges are predicated in part on the observation that sulfur isotope results for the microlaminated sediments of the deep Black Sea as compared to water-column $\delta^{34}S_{HS}$- data (Muramoto et al., 1991; Calvert et al., 1996; Lyons, 1997), in combination with DOP trends (Lyons and Berner, 1992; Lyons, 1997) and framboid size distributions (Wilkin et al., 1996, 1997), suggest that most of the pyrite forms very rapidly within the chemocline region of the anoxic–sulfidic water column (see also Cutter and Kluckhohn, 1999). Diagenetic additions account for perhaps only 10% to 20% over 10^3-year time scales, despite readily available HS^- in the pore waters (Lyons and Berner, 1992; Lyons, 1997). Collectively, this pyrite formation results in DOP values in near-surface Black Sea sediments that are as high as 0.70 and reach 0.78 by 14 cm depth, which are generally within the DOP realm for anoxic to anoxic–sulfidic deposition defined by Raiswell et al. (1988), despite recording rapid pyrite formation rather than prolonged exposure to dissolved sulfide.

In contrast to the deep basin, euxinic deposits along the margin of the Black Sea are characterized by extreme rates of sediment accumulation (approaching 0.8 cm $year^{-1}$) and show low to intermediate DOP values (0.32 to 0.47) that fall within the aerobic region of the Raiswell et al. (1988) DOP scheme (Lyons, 1992, 1997; Hurtgen et al., 1999). These low values occur despite the sulfidic bottom waters and persistent exposure of the sediments over several decades to levels of pore-water sulfide (from ~ 40 to 2000 μM) that can be substantially higher than those observed within the deep euxinic water column (300 to 400 μM) and within the pore waters of the deep-basin sediments (~ 200 to 700 μM) (Sweeney and Kaplan, 1980; Fry et al., 1991; Lyons, 1992, 1997; Lyons and Berner, 1992; Hurtgen et al., 1999). Low to intermediate DOP values are also observed at the oxic FOAM site in Long Island Sound to depths of at least 260 cm despite persistent exposure to HS^- concentrations reaching 6 mM (Canfield et al., 1992). Collectively, these and related observations have confirmed that extents of pyritization (DOP), while being linked to depositional redox, have more to do with the nature of the iron reservoir than time of exposure to high concentrations of HS^-. Furthermore, these relationships confirm that the HCl extraction is an overestimation of the most readily reactive Fe phases (Canfield et al., 1992; Raiswell et al., 1994; Raiswell and Canfield, 1996, 1998).

A recent model argues that DOP values are largely controlled by the relative proportions of Fe delivered with (1) detrital sediment (e.g., Fe oxides and silicates) and (2) as a fraction that varies in magnitude and is decoupled from the local detrital flux through the scavenging of dissolved Fe from the water column during syngenetic pyrite formation (Canfield et al.,

Table 2
Comparative details of sulfate vs. sulfide diffusion models—a summary of contrasting responses to post-glacial sea-level rise (see text for additional details)

Black Sea Model

- Isolated silled basin; freshwater deposition during last glacial sea-level lowstand.
- Freshwater host sediment initially sulfate-limited.
- Reactive Fe and C_{org} (or CH_4; Jørgensen et al., 2001) initially available in host sediment.
- Increasing marine influence during sea-level rise above level of sill leads to SO_4^{2-} diffusion into freshwater deposits from oxic, brackish water column.
- Diagenetic S_{py} overprint via in situ HS^- production in SO_4^{2-} restricted pore-water reservoir—SO_4^{2-} consumption (via bacterial reduction) outpaces diffusional replenishment (consistent with SO_4^{2-} limited source from brackish overlying water).
- High $\delta^{34}S_{py}$ values of overprinting pyrite approximate initial $\delta^{34}S_{sulfate}$ value.
- Suggests dominantly SO_4^{2-} diffusion before onset of water-column anoxia (and thus before water-column HS^- production)—consistent with independent constraints on basin evolution over last glacial–interglacial transition.
- C_{org}/S_{py} ratios shifted from freshwater to marine values by pyrite overprint.
- Summary: Pyrite overprint represents SO_4^{2-} diffusion marking basin evolution from freshwater to oxic, C_{org}-poor marine (brackish) conditions—later onset of euxinic water column.
- Other examples: Kau Bay, Indonesia; Baltic Sea.

Cariaco Basin Model

- Silled basin, oxic marine deposition during last glacial sea-level lowstand (nutrient-deficient surface waters).
- Oxic marine host sediment initially C_{org}-limited.
- SO_4^{2-} and reactive Fe initially available in host sediment.
- Sea-level rise results in increased nutrient inputs to photic zone and thus greater primary production; corresponding increases in respiration in restricted basin result in euxinic deep waters.
- "Rapid" onset of euxinic water column results in downward diffusion of HS^- from Fe-limited water column and microlaminated sediments.
- Diffusing sulfide reacts with readily available reactive Fe in sediments to form abundant pyrite.
- $\delta^{34}S_{py}$ values of overprinted pyrite initially approximate $\delta^{34}S_{HS^-}$ values of euxinic water column.
- As Fe is consumed in bioturbated clay, pyrite front advances downward.
- Overlying HS^- source evolves (in restricted pore-water reservoir of basal microlaminated sediments) so that $\delta^{34}S_{py}$ values increase downward within diffusionally overprinted zone.
- Transition from gray to reddish-brown clay marks downward limit of HS^- diffusion.
- C_{org}/S_{py} ratios shifted from normal (oxic) marine to euxinic marine values by pyrite overprint.
- Summary: Pyrite overprint represents HS^- diffusion marking "rapid" transition from oxic, C_{org}-deficient marine conditions to euxinic marine setting.

Table 2 (*continued*)

Cariaco Basin Model

- Other example: Analogous pyrite overprints observed beneath Mediterranean sapropels—HS^- production within C_{org}-rich sapropel out-competes Fe supply and thus migrates via diffusion and reacts within Fe-rich but C_{org}-poor underlying sediment. Low $\delta^{34}S_{py}$ values reflect "open" system behavior in terms of balance between SO_4^{2-} consumption and availability/replenishment.

1996; Lyons, 1997; Raiswell and Canfield, 1998; Raiswell et al., 2001; Werne et al., 2002). In other words, a percentage of the detrital Fe will be reactive on short time scales within the water column and sediments, but because the HCl extraction includes phases that are reactive only on time scales of $\geq 10^2$ years, low to intermediate DOP values can be observed despite exposure to an abundance of HS^- over comparatively long time periods. However, if pyrite forms within the water column by (1) reacting with the highly reactive fraction of the detrital Fe and (2) by scavenging dissolved Fe that is independent of the local detrital flux, the total pyrite Fe reservoir is augmented by the scavenging without a corresponding increase in the unreacted, detrital, HCl-extractable fraction. In simplified terms, Fe scavenging can result in higher DOP values, higher ratios of highly reactive ($Fe_D + Fe_{py}$) to total Fe, and higher Fe_T/Al ratios relative to the detrital source (Canfield et al., 1996; Lyons, 1997; Raiswell and Canfield, 1998; Yarincik et al., 2000a; Raiswell et al., 2001; Werne et al., 2002).

In the modern Black Sea, which provides a template for interpretations of the Cariaco Basin, carbonate-rich, microlaminated (Unit 1) sediments of the deep basin have Fe_T/Al ratios that are up to ~ 2.5 times greater than the siliciclastic-dominated euxinic deposits of the basin margin: 0.5 to 0.6 for the margin vs. ~ 0.7 to 1.2 for the deep basin (T.W. Lyons, unpublished results; see also Wilkin and Arthur, 2001). Again, these basin-margin (upper-slope) sediments are accumulating at ~ 0.8 cm year^{-1} (relative to ~ 0.02 cm year^{-1} for the deep basin) and have Fe_T/Al ratios approximating those of the oxic shelf. Our ongoing work suggests that these spatial differences in Fe_T/Al ratios are far greater than those observed across modern open ocean basins, where transport-related phenomena (physical sorting/fractionation processes) alone can result in increasing Fe_T/Al ratios with increasing distance from the continents.

The present study of the Cariaco Basin highlights Fe trends at a single location, thus minimizing spatial (transport) artifacts other than those related to sea-level change; however, potential (tectonically or climatically controlled) temporal variations in input remain a complicating possibility.

Details regarding the origin of the "extra" Fe (i.e., a basin-scale mass balance of the externally sourced Fe) and the possible role of biogenic grains as sites of enhanced sulfate reduction, pyrite formation, and thus Fe scavenging within the water column are discussed elsewhere (Raiswell and Canfield, 1998; Raiswell et al., 2001; Wijsman et al., 2001). For the purpose of the present Cariaco Basin study, however, the key element of this model is that Fe_T/Al ratios can be elevated in euxinic settings through water-column pyrite formation. Ultimately, the magnitude of this enrichment is a product of the balance between rates of detrital input and the "rain" rate of scavenged Fe. Under conditions of very high detrital (siliciclastic) input, the scavenged Fe can be swamped by the detrital fraction, thus resulting in DOP values that look more like oxic deposits and Fe_T/Al ratios that approximate the continental (detrital) sediment flux. As a result of these relationships, DOP values and Fe_T/Al ratios can vary laterally and temporally beneath an anoxic–sulfidic water column as a function of varying rates of detrital sedimentation. In theory, however, any Fe_T/Al ratio elevated beyond the scatter in the continental baseline could be attributed to euxinic conditions, regardless of sedimentation rates—DOP is a useful but less sensitive indicator of paleoredox. Rates of pyrite formation in the water column and the nature (reactivity) of the detrital flux can vary but are viewed as secondary controls relative to those linked to the presence or absence of a euxinic water column and the rates of detrital sedimentation.

It is tempting to suggest that the Fe arguments above unnecessarily complicate the straightforward redox-dependent DOP story of Raiswell et al. (1988). In reality, DOP is not a simple proxy. As suggested by Raiswell et al., high DOP values, which vary somewhat from basin to basin (or within a basin) as a function of rates of siliciclastic accumulation and syngenetic pyrite formation, uniquely delineate a sulfidic water column. Low values argue convincingly for oxic deposition with low associated C_{org} accumulation. By contrast, intermediate values (often in the range of $\sim 0.3-0.6$) suggest one of three possibilities: (1) oxic deposition, and thus purely diagenetic pyrite formation, with appreciable associated concentrations of C_{org}; (2) depositional conditions vacillating between oxic and euxinic; and (3) persistently euxinic deposition where the syngenetic pyrite flux and its associated scavenged Fe are swamped by continental sediment inputs.

6.3.2. Iron in the Cariaco Basin

Variance in the balance between delivery of scavenged and detrital Fe explains the broad range of DOP values (0.55–0.93) described by Raiswell et al. (1988) for the anoxic to anoxic–sulfidic end members at many different ancient localities. This balance also explains the relationship between the DOP values and Fe_T/Al ratios observed in the Cariaco Basin and those of other euxinic settings. (Values for DOP and the Fe_T/Al ratios generally track each other [compare Figs. 7 and 8], including the abrupt increase observed below 5.3 mbsf.) The microlaminated deposits in the Cariaco are intermediate in terms of siliciclastic delivery relative to the Black Sea end members described above. Sedimentation rates provide an approximation of siliciclastic delivery, and DOP values and Fe_T/Al ratios can, therefore, be related to bulk sedimentation rates and their spatial gradients beneath the euxinic portion of the water column. Nevertheless, high and variable biogenic contributions (opal and $CaCO_3$) in both the Cariaco Basin and the Black Sea suggest that siliciclastic accumulation rates (g m^{-2} $year^{-1}$) would be a better approach. Uncertainties regarding opal contents and porosities, as well as the extreme variability in many of the parameters for the Cariaco sediments, make it difficult to calculate precise siliciclastic accumulation rates. However, opal estimates based on correlative cores (L.C. Peterson, unpublished results), along with published $CaCO_3$ contents (e.g., Werne et al., 2000b), allow us to bracket the range of possible siliciclastic accumulation rates (Table 3). Regardless of the opal contents and porosities reasonably assumed for the Cariaco sediments, siliciclastic delivery is clearly intermediate with respect to the Black Sea end members.

As predicted from our model, and assuming some degree of uniformity in interbasinal syngenetic pyrite formation, the DOP values of the Cariaco sediments

Table 3
Calculations of siliciclastic accumulation rates for the Black Sea and Cariaco Basin

Core location	Water depth (m)	Sedimentation rate (cm ky^{-1})	Grain density (g cm^{-3})	Porosity	Total sediment accumulation rate (g m^{-2} $year^{-1}$)	Siliciclastic content (%)	Siliciclastic accumulation rate (g m^{-2} $year^{-1}$)
Black Sea Station 9	2087	15.9	2.4	0.90	38.2	45.5	17.4
Black Sea Station 14	2218	15.8	2.4	0.90	37.9	49.8	18.9
Black Sea Station 15	198	770	2.5	0.90	1925.0	86.5	1665.1
Cariaco Basin	~ 900	44.8 (6.5 m/14.5 ky,	~ 2.4[a]	0.90	107.5	40	43.0
ODP Site 1002		assuming linear				55	59.1
(microlaminated		sedimentation rare)				70	75.3
interval < 6.5 mbsf)				0.70	322.6	40	129.0
						55	177.4
						70	225.8
				0.50	537.6	40	215.0
						55	295.7
						70	376.3

Black Sea results are modified from Calvert et al. (1991; see also Lyons, 1991, 1992, 1997; Lyons and Berner, 1992) and Anderson et al. (1994) for Station 15. Cariaco results are calculated based on high, low, and mean estimates for porosity and siliciclastic content (see Section 6.3.2 for additional details). Siliciclastic contents for the Cariaco Basin are estimated using available data for opal, $CaCO_3$, and C_{org} contents. These estimates for siliciclastic abundance are consistent with those calculated by Yarincik et al. (2000b) from Ti and Al contents.

[a] Estimated based on roughly similar C_{org} contents in Black Sea (Unit 1) and Cariaco Basin (< 6.5 mbsf).

(mean: 0.55 ± 0.03, $n = 47$) are also intermediate—reflecting the magnitude of the detrital Fe contribution relative to the delivery of scavenged Fe that is decoupled from the local detrital flux. The DOP values increase from surface values around 0.50 to a maximum of 0.58 by 1.25 mbsf. Other than this downcore increase in the upper layers and a sharp increase from 5.3 to 5.9 mbsf, which may reflect increased water-column pyrite formation or dramatic reduction of the detrital influx, the DOP values are comparatively uniform over much of the microlaminated interval. One way to interpret this DOP relationship is a 10% increase in iron sulfidation during diagenetic pyrite formation in the upper layers which augments a largely syngenetic reservoir. Given the nonsteady-state nature of deposition of the most recent microlaminated interval in the Cariaco Basin (Peterson et al., 1991; Hughen et al., 1996a,b, 1998; Lin et al., 1997; Shipboard Scientific Party, 1997; Werne et al., 2000b), however, syngenetic inputs augmented by systematic diagenetic pyrite formation in the upper portion of the core may be an oversimplified view (compare the mass balance approach of Werne et al., 2003, this volume).

In contrast to preliminary data published in Yarincik et al. (2000a, their Fig. 3)—where an elevated Fe_T/Al ratio is not observed in the uppermost microlaminated deposits relative to the subjacent bioturbated (oxic) sediments—the present results show generally elevated Fe_T/Al ratios in the microlaminated sediments below the upper ~ 100 cm (Fig. 7). As outlined above, this enrichment likely reflects the scavenging of Fe in the euxinic water column during pyrite formation, as is supported by the sulfur geochemical evidence, including the $\delta^{34}S$ relationships (see also Werne et al., 2003, this volume). The Fe_T/Al ratios are generally elevated by roughly 10% to 20% relative to the bioturbated sediments, which is greater than the euxinic (vs. oxic) enrichment observed along the margin of the Black Sea—where sedimentation is very rapid—but is far below the percent enrichment observed in the more siliciclastically starved Black Sea basin interior. As for the DOP, the intermediate Fe_T/Al ratios in the Cariaco relative to the end members described from the Black Sea reflect the intermediate rates of siliciclastic input and thus the relative degrees to which the scavenged (siliciclastic-independent) component is swamped by detrital Fe_T/Al ratios. The upwardly decreasing but scattered Fe_T/Al ratios over the upper 100 cm, with minima approximating those of the underlying oxic sediments, reflect a temporal increase in detrital sedimentation and/or a decrease in syngenetic pyrite formation toward the present. Either of these mechanisms would explain the

similar upcore decrease in DOP observed over the upper 100 cm (Fig. 8).

Contrary to the subtle euxinic enrichment in Fe_T/Al ratio during interglacial deposition described here, Yarincik et al. (2000a) reported a general trend toward Fe enrichment during the oxic conditions of the glacial intervals of the ~580-ky record. They further noted, however, that the Fe_T/Al ratios tend to be statistically noncoherent or only weakly coherent with respect to independent proxies for depositional redox on glacial–interglacial time scales. Again, the "weakness" of the scavenged Fe signal in the Cariaco reflects the large siliciclastic flux compared, for example, to the deep Black Sea—i.e., the terrigenous inventory in the Cariaco is a larger fraction of the total Fe reservoir. Such a large and variable siliciclastic input would impact the relative strength of the signal over time.

Finally, the Fe scavenging model outlined above should result in not only potentially higher DOP values and Fe_T/Al ratios under euxinic conditions but also elevated ratios of highly reactive ($Fe_D + Fe_{py}$) to total Fe. The Fe scavenging during pyrite formation in the water column drives the ratio up (the scavenged Fe is, by definition, highly reactive) relative to the Fe reservoir delivered locally with the detrital sediment (Raiswell and Canfield, 1998; Raiswell et al., 2001). Raiswell and Canfield (1998) reported ratios of $Fe_D + Fe_{py}$ to total Fe from the same microlaminated samples from the Cariaco Basin. These ratios are generally intermediate between those of oxic continental shelves and the deep-water, microlaminated sediments of the Black Sea, which is predicted given the relative siliciclastic fluxes for the Cariaco and Black Sea.

6.4. Controls of molybdenum distribution

The mechanisms by which Mo is enriched in organic-rich, black shale environments have been discussed at length in the literature. One debate centers on the relative contributions of water-column scavenging vs. enrichment via diffusion across the sediment–water interface. This distinction is critical if we hope to use Mo/Al ratios that are elevated far above average continental levels as a proxy for truly euxinic conditions (i.e., as indicative of HS^- in the water column). A central theme running through these arguments is the presence of high concentrations of dissolved sulfide. Questions arise, however, when addressing whether the high HS^- levels must occur uniquely in the sediment or the water column or whether both may effect the enrichment, thus allowing the possibility for Mo accumulation through diffusion into organic-rich (and thus sulfide-rich) sediments that commonly occur under hypoxic to anoxic but not necessarily euxinic water columns.

The properties of the Cariaco sediments indirectly illuminate mechanistic details for Mo enrichment in organic-rich sediments. First, Mo/Al ratios are high in the microlaminated zone (see also Dean et al., 1999) and *generally* track the concentration of C_{org} (Fig. 9). Such covariance, albeit subtle, could reflect (1) a true physicochemical coupling between deposition of the two phases (i.e., Mo scavenging by organic matter; e.g., Coveney et al., 1991; Helz et al., 1996); (2) the importance of HS^- in Mo accumulation (Crusius et al., 1996; Helz et al., 1996; Erickson and Helz, 2000; Zheng et al., 2000; Adelson et al., 2001), wherein high concentrations of C_{org} result in greater bacterial HS^- generation in the sediment or the water column (Dean et al., 1999); or (3) scavenged seawater Mo (which is independent of the local detrital flux) and C_{org} deposition that are geochemically decoupled but mimic covariance by similarly responding to time-varying dilution by siliciclastic sedimentation with low (continental) Mo/Al ratios. The latter is refuted by the corresponding trend for Fe_T/Al (Fig. 7), which fails to suggest the sympathetic variations with C_{org} concentrations and Mo/Al ratios. Covariation would be predicted for detrital dilution effects alone. Furthermore, maxima in Mo accumulation ($\mu g\ Mo\ cm^{-2}\ year^{-1}$; Dean et al., 1999), which are independent of siliciclastic dilution, generally correlate with the peak Mo/Al ratios in Fig. 9. Interestingly, rates of C_{org} (Werne et al., 2000b) and Mo accumulation, if anything, are inversely related, suggesting that HS^- generating potential as related to C_{org} *concentration* may be the critical factor.

Ratios of Mo to Al are low (i.e., at average continental levels) and independent of C_{org} concentrations in both the gray and reddish-brown bioturbated clays, despite the evidence (S_{py} concentrations) for high pore-water HS^- within the uppermost (gray) oxic deposits resulting from the diffusional overprint. Interestingly, Mo/Al ratios do not track S_{py} concentrations in either the oxic or euxinic deposits, which challenges

previous assertions that Mo deposition is linked to pyrite accumulation (Huerta-Diaz and Morse, 1992).

There is little evidence for Mo enrichment via diffusion into the sulfur-rich (gray, oxic) sediments. Here, Mo/Al ratios fall within the range of 10^{-5}, which are roughly average-shale (continental) values (Taylor and McLennan, 1985) lacking syngenetic or diagenetic enrichment. (The gray clays show Mo/Al ratios that are about a factor of two higher than in the underlying reddish-brown clay but are substantially lower than the 10^{-3} range observed for the microlaminated sediments). This lack of appreciable enrichment could reflect the critical but poorly constrained direct role played by organic matter in Mo sequestration, but the comparatively low C_{org} concentrations in the gray clay show no relationship to Mo distributions despite the presence of high amounts of sulfide in the system (Fig. 9). These observations are seemingly inconsistent with models favoring Mo enrichment by reaction at or diffusion across the sediment–water interface into HS^--rich sediments (i.e., diagenetic pathways; Francois, 1988; Emerson and Huested, 1991; Crusius et al., 1996; Zheng et al., 2000; Adelson et al., 2001; see also Erickson and Helz, 2000)—rather than possible water-column scavenging (this study; Helz et al., 1996)—as the principal mechanism for Mo enrichment in low-oxygen/high-sulfide settings, including but not limited to euxinic waters.

One possible explanation for the striking contrast in Mo enrichment in the microlaminated sediments vs. the gray and reddish-brown oxically deposited muds is the requirement for a sulfidic water column, in which particulates can scavenge Mo (Helz et al., 1996). The model of Helz et al. (1996) argues that molybdate begins to convert to thiomolybdate at a critical value (switchpoint) for a_{HS^-}, which then becomes reactive to particles that include sulfurized organic matter. (Pathways and the timing of organic-matter sulfurization in the Cariaco Basin are explored in Werne et al. (2003)). There is nothing about this model, however, that requires this process to occur in the water column, and past studies in the Black Sea and Saanich Inlet (Francois, 1988; Crusius et al., 1996) have relied on the absence of Mo enrichment in the sediment traps to argue for mineralization mechanisms within sulfidic pore waters rather than in the water column.

Sediment trap results from the Cariaco are unfortunately too preliminary to rule out water-column processes. Initial results from trap samples collected immediately above and below the chemocline in an ongoing study (R.W. Murray and R.C. Thunell, unpublished results) show Mo concentrations that are actually below continental (average shale) values and thus the concentrations observed for the gray and reddish-brown sediments. While this may argue against water-column scavenging, the sulfide concentrations (and thus activities) immediately below the O_2/H_2S interface (de Baar et al., 1988; Fry et al., 1991) are well below the sulfide switchpoint of Helz et al. (1996) required for production of thiomolybdate. Whether Mo scavenging occurs deeper in the sulfidic water column is still unknown, although the sulfide concentrations of <100 μM may be inadequate. If Mo enrichment occurs only via diffusion into the sulfidic pore waters, however, it is curious that the highly sulfide-overprinted bioturbated sediments show no enhanced Mo concentrations—the kick in elevated Mo/Al ratios corresponds precisely with the onset of microlaminated deposition. The role of organic matter may be the key ingredient as a substrate for thiomolybdate scavenging and/or the controlling factor in attaining the threshold HS^- activity. Regardless, it is risky to extrapolate modern water-column chemistry as a simple template for paleoenvironmental conditions in a temporally dynamic depositional system. The persistence of lamination, the comparatively low and uniform $\delta^{34}S_{py}$ values in the laminated deposits, and the elevated Fe_T/Al ratios all argue for continuously euxinic conditions over the ~14.5 calendar ky period of Mo enrichment but provide few specifics about the quantity and quality of the organic matter and related HS^- concentrations in the water column and sediments over time. The subtle downcore increase in Fe_T/Al ratios (and DOP) over the upper ~1.0 mbsf could, however, reflect higher water-column sulfide concentrations in the past. Accumulation of Mo in the Cariaco Basin over the last ~24 and ~580 calendar ky is further addressed in Dean et al. (1999) and Yarincik et al. (2000a), respectively.

7. Paleoenvironmental implications

The modern euxinic conditions of the Cariaco Basin and, in particular, the abrupt juxtaposition of oxic and euxinic sediments at ~14.5 calendar ka BP

are ideal for the development and refinement of paleoredox proxies used in paleoenvironmental reconstructions of ancient fine-grained siliciclastic sequences. Invariant ^{34}S-depleted $\delta^{34}S_{py}$ values in the microlaminated sediments of the modern euxinic Black Sea (Muramoto et al., 1991; Calvert et al., 1996; Lyons, 1997; Wilkin and Arthur, 2001) and ancient analogs (Anderson et al., 1987; Fisher and Hudson, 1987; Beier and Hayes, 1989; Werne et al., 2002) are commonly taken as indicators of dominantly water-column pyrite formation, reflecting the large size and uniform nature of the *water-column* sulfate and sulfide reservoirs. This syngenetic pyrite formation is corroborated by independent assessments of pyrite framboid size distributions (Wilkin et al., 1996, 1997; Wignall and Newton, 1998). While the specifics of pyrite formation in the Cariaco Basin are complex, given the very nonsteady-state properties of deposition and diagenesis, the sulfur isotope relationships of the pyrite within the microlaminated sediments are consistent with a substantial syngenetic contribution (this study; Werne et al., 2003, this volume). Degree-of-pyritization values are mostly intermediate (in the 0.50–0.60 range), which by the convention of Raiswell et al. (1988) would suggest an oxygenated water column. However, a refined view of DOP reveals that these intermediate values are expected under euxinic deposition in the presence of a comparatively large, diluting siliciclastic flux (this study; Canfield et al., 1996; Lyons, 1997; Raiswell and Canfield, 1998; Raiswell et al., 2001; Werne et al., 2002). Similarly, Fe_T/Al ratios are elevated above the oxic (continental) level, suggesting Fe scavenging through syngenetic pyrite formation in the euxinic water column (i.e., reactive Fe augmentation that is decoupled from the local siliciclastic flux). The Cariaco data, along with those from the Black Sea and ancient black shales, indicate that Fe_T/Al ratios can be used as an unambiguous indicator of a sulfidic water column, as well as a proxy for spatially and temporally varying clastic influx across euxinic basins (this study; Lyons, 2000; Wilkin and Arthur, 2001; Werne et al., 2002).

The S_{py} overprint in the oxic sediments caused by diffusion following the onset of euxinic deposition highlights the care necessary in using C_{org}–S_{py} relationships in paleoenvironmental reconstructions. Without the context of the diffusional secondary overprint (and careful sedimentological and paleoecological observations), the very high levels of S_{py} relative to the amount of C_{org} present would falsely suggest euxinic depositional conditions (i.e., the low C_{org}/S_{py} ratios that sometimes characterize euxinic conditions; Berner and Raiswell, 1983; Leventhal, 1983; Raiswell and Berner, 1985; compare Calvert and Karlin, 1991; Lyons and Berner, 1992), just as pyrite overprints in the Black Sea, the Baltic Sea, and Kau Bay (Indonesia) could lead to spurious marine interpretations for the freshwater deposits (Middelburg, 1991; Middelburg et al., 1991; Leventhal, 1995; Sternbeck and Sohlenius, 1997). Despite the sulfur overprint in the Cariaco Basin, the onset of elevated Mo/Al ratios corresponds precisely with the onset of euxinic deposition; the oxically deposited sediments show essentially continental Mo/Al ratios little affected by the pronounced secondary effect. Overall, geochemical relationships in the sediments of the Cariaco Basin have obvious implications for the interpretation of paleoredox in ancient sequences, particularly when combined in an integrated, multiproxy investigation. The utility of this collective sulfur/trace-metal approach is well documented in a recent study of Devonian shales from western New York (Werne et al., 2002). Despite the patterns observed in the Cariaco, however, it is unlikely that Mo/Al ratios provide a universally valid proxy for the presence of hydrogen sulfide in ancient water columns. Fe_T/Al ratios show more promise in that regard.

8. Summary and conclusions

Recent drilling in the Cariaco Basin revealed a roughly 580-ky record of deposition that alternated between oxic and anoxic conditions on glacial–interglacial time scales (Shipboard Scientific Party, 1997; Peterson et al., 2000). The transition between the persistently euxinic (anoxic–sulfidic) bottom waters of the last ~ 14.5 ky and the preceding oxic bottom waters of the last glacial episode was abrupt. The present study of this paleoredox transition and the overlying euxinic deposits suggests the following.

(1) Pyrite formation in the microlaminated, euxinic sediments is Fe-limited. Downcore trends for pyrite concentrations, degrees-of-pyritization, and

iron/aluminum ratios—in combination with sulfur isotope constraints—confirm that a substantial portion of the pyrite in the microlaminated sediments formed within the euxinic water column. However, estimates for the relative proportions of diagenetic vs. syngenetic pyrite vary. It is difficult to uniquely deconstruct the relative proportions of syngenetic vs. diagenetic pyrite in the microlaminated interval given the complex, nonsteady-state history of deposition and (perhaps) pyrite formation and the uncertainties in age models that are required for alternative approaches based on accumulation rates (Werne et al., 2003, this volume). The proportions would ultimately reflect the availability of dissolved sulfide in the water column and the distribution of Fe that is reactive on short time scales.

(2) Pyrite formation in the underlying oxic sediments was controlled initially by organic-carbon availability and, for the uppermost bioturbated layers, by "secondary" Fe limitation linked to HS^- diffusion from the overlying Fe-limited, organic-carbon-rich euxinic sediments and water column. This transition from oxic marine to euxinic marine conditions manifests in pyrite overprints that are strongly ^{34}S-depleted relative to those in temporally analogous but hydrographically distinct marine settings elsewhere in the world, such as the Black Sea (i.e., silled basins where the last glacial–interglacial transition is marked instead by transitions from freshwater to oxic marine deposition followed by euxinic conditions).

(3) Ratios of total Fe to Al that are slightly elevated above continental levels and the intermediate degrees-of-pyritization in the microlaminated sediments of the Cariaco Basin are consistent with an iron reservoir controlled by Fe scavenging during water-column (syngenetic) pyrite formation in combination with "intermediate" rates of Fe-bearing siliciclastic sedimentation. Cariaco Fe_T/Al ratios and DOP values lie between those of the siliciclastic accumulation-rate end members in the euxinic Black Sea that bracket accumulation rates in the Cariaco. These intermediate values confirm that both parameters ultimately reflect the balance between syngenetic pyrite formation and temporally and spatially varying detrital sedimentation in modern and, by inference, ancient oxygen-deficient settings. The Cariaco data corroborate that Fe_T/Al ratios can be used as an unambiguous indicator of sulfidic water columns, as well as a proxy for spatial and temporal gradients in clastic influx within euxinic basins.

(4) Trends for Mo/Al ratios in the Cariaco Basin record clear Mo enrichment in the microlaminated sediments (relative to the continental levels recorded by the oxic sediments). Organic matter plays a role by enhancing HS^- production and/or by providing a (sulfurized?) substrate for thiomolybdate scavenging. Our study provides no direct evidence for significant Mo enrichment via diffusion into HS^--rich pore waters despite the heavily sulfide overprinted sediments in the upper portion of the bioturbated zone. However, the importance of high sulfide concentrations *within the water column* as an essential ingredient for enhanced Mo sequestration requires further investigation.

Acknowledgements

The senior author acknowledges with gratitude his co-editors Chuanlun Zhang and Chris Romanek and the editors and staff of *Chemical Geology* for their encouragement in assembling this special issue. The authors also thank the many ODP staff members, both shipboard and shore-based, for a successful cruise. The Leg 165 Shipboard Scientific Party, in particular Graham Pearson, contributed significantly to shipboard sediment processing and pore-water data generation. Larry Peterson was the principal proponent in proposing and accomplishing the Cariaco drilling. Kim Keel provided expert assistance in the MU lab. Mike Formolo, Jon Fong, Steve Studley, and the Indiana University stable isotope facility are acknowledged for their contributions to the S isotope portion of this study. Details of the iron model were strongly influenced by collaborations and conversations with Don Canfield and Rob Raiswell. Partial financial support was provided to TWL and RWM by JOI-USSSP. Funds for this research were also provided to TWL by NSF grant EAR-9875961. NSF-EAR provided partial funds for the development and support of the IU sulfur stable isotope facility (TWL co-PI). This contribution

benefited significantly from the insightful reviews of Rob Raiswell, Rick Wilkin, and one anonymous reader. **[EO]**

References

Adelson, J.M., Helz, G.R., Miller, C.V., 2001. Reconstructing the rise of recent coastal anoxia; molybdenum in Chesapeake Bay sediments. Geochim. Cosmochim. Acta 65, 237–252.

Anderson, T.F., Kruger, J., Raiswell, R., 1987. C–S–Fe relationships and the isotopic composition of pyrite in the New Albany Shale of the Illinois Basin, U.S.A. Geochim. Cosmochim. Acta 51, 2795–2805.

Anderson, R.F., Fleisher, M.Q., Le Huray, A.P., 1989a. Concentration, oxidation state, and particulate flux of uranium in the Black Sea. Geochim. Cosmochim. Acta 53, 2215–2224.

Anderson, R.F., Le Huray, A.P., Fleisher, M.Q., Murray, J.W., 1989b. Uranium depletion in Saanich Inlet sediments, Vancouver Island. Geochim. Cosmochim. Acta, 2205–2213.

Anderson, R.F., Lyons, T.W., Cowie, G.L., 1994. Sedimentary record of a shoaling of the oxic/anoxic interface in the Black Sea. Mar. Geol. 116, 373–384.

Arthur, M.A., Dean, W.E., 1998. Organic-matter production and preservation and evolution of anoxia in the Holocene Black Sea. Paleoceanography 13, 395–411.

Arthur, M.A., Sageman, B.B., 1994. Marine black shales: a review of depositional mechanisms and significance of ancient deposits. Annu. Rev. Earth Planet. Sci. 22, 499–551.

Bacon, M.P., Brewer, P.G., Spencer, D.W., Murray, J.W., Goddard, J., 1980. Lead-210, polonium-210, manganese and iron in the Cariaco Trench. Deep-Sea Res. 27A, 119–135.

Beier, J.A., Hayes, J.M., 1989. Geochemical and isotopic evidence for paleoredox conditions during deposition of the Devonian–Mississippian New Albany Shale, southern Indiana. Geol. Soc. Amer. Bull. 101, 774–782.

Berner, R.A., 1970. Sedimentary pyrite formation. Am. J. Sci. 268, 1–23.

Berner, R.A., 1982. Burial of organic carbon and pyrite sulfur in the modern ocean: its geochemical and environmental significance. Am. J. Sci. 282, 451–473.

Berner, R.A., 1984. Sedimentary pyrite formation: an update. Geochim. Cosmochim. Acta 48, 605–615.

Berner, R.A., Raiswell, R., 1983. Burial of organic carbon and pyrite sulfur in sediments over Phanerozoic time: a new theory. Geochim. Cosmochim. Acta 47, 855–862.

Berner, R.A., Baldwin, T., Holdren, G.R., 1979. Authigenic iron sulfides as paleosalinity indicators. J. Sediment. Petrol. 49, 1345–1350.

Breit, G.N., Wanty, R.B., 1991. Vanadium accumulation in carbonaceous rocks: a review of geochemical controls during deposition and diagenesis. Chem. Geol. 91, 83–97.

Calvert, S.E., Karlin, R.E., 1991. Relationships between sulphur, organic carbon, and iron in the modern sediments of the Black Sea. Geochim. Cosmochim. Acta 55, 2483–2490.

Calvert, S.E., Pedersen, T.F., 1993. Geochemistry of recent oxic and anoxic marine sediments: implications for the geological record. Mar. Geol. 113, 67–88.

Calvert, S.E., Karlin, R.E., Toolin, L.J., Donahue, D.J., Southon, J.R., Vogel, J.S., 1991. Low organic carbon accumulation rates in Black Sea sediments. Nature 350, 692–695.

Calvert, S.E., Thode, H.D., Yeung, D., Karlin, R.E., 1996. A stable isotope study of pyrite formation in the Late Pleistocene and Holocene sediments of the Black Sea. Geochim. Cosmochim. Acta 60, 1261–1270.

Canfield, D.E., 1989. Reactive iron in marine sediments. Geochim. Cosmochim. Acta 53, 619–632.

Canfield, D.E., Raiswell, R., Westrich, J.T., Reaves, C.M., Berner, R.A., 1986. The use of chromium reduction in the analysis of reduced inorganic sulfur in sediments and shales. Chem. Geol. 54, 149–155.

Canfield, D.E., Raiswell, R., Bottrell, S., 1992. The reactivity of sedimentary iron minerals toward sulfide. Am. J. Sci. 292, 659–683.

Canfield, D.E., Lyons, T.W., Raiswell, R., 1996. A model for iron deposition to euxinc Black Sea sediments. Am. J. Sci. 296, 818–834.

Chanton, J.P., Martens, C.S., 1985. The effects of heat and stannous chloride addition on the active distillation of acid volatile sulfide from pyrite-rich marine sediment samples. Biogeochemistry 1, 375–383.

Colodner, D., Edmond, J., Boyle, E., 1995. Rhenium in the Black Sea: comparison with molybdenum and uranium. Earth Planet. Sci. Lett. 131, 1–15.

Coveney Jr., R.M., Watney, W.L., Maples, C.G. 1991. Contrasting depositional models for Pennsylvanian black shale discerned from molybdenum abundances. Geology 19, 147–150.

Crusius, J., Calvert, S., Pedersen, T., Sage, D., 1996. Rhenium and molybdenum enrichments in sediments as indicators of oxic, suboxic and sulfidic conditions of deposition. Earth Planet. Sci. Lett. 145, 65–78.

Cutter, G.A., Kluckhohn, R.S., 1999. The cycling of particulate carbon, nitrogen, sulfur and sulfur species (iron monosulfide, greigite, pyrite, and organic sulfur) in the water columns of Framvaren Fjord and the Black Sea. Mar. Chem. 67, 149–160.

Dean, W.E., Arthur, M.A., 1989. Iron–sulfur–carbon relationships in organic-carbon-rich sequences: I. Cretaceous Western Interior seaway. Am. J. Sci. 289, 708–743.

Dean, W.E., Piper, D.Z., Peterson, L.C., 1999. Molybdenum accumulation in Cariaco Basin sediment over the past 24 k.y.: a record of water-column anoxia and climate. Geology 27, 507–510.

de Baar, H.J.W., German, C.R., Elderfield, H., van Gaans, P., 1988. Rare earth element distributions in anoxic waters of the Cariaco Trench. Geochim. Cosmochim. Acta 52, 1203–1219.

Ding, T., Valkiers, S., Kipphardt, H., De Bièvre, P., Taylor, P.D.P., Gonfiantini, R., Krouse, R., 2001. Calibrated sulfur isotope abundance ratios of three IAEA sulfur isotope reference materials and V-CDT with a reassessment of the atomic weight of sulfur. Geochim. Cosmochim. Acta 65, 2433–2437.

Dorta, C.C., Rona, E., 1971. Geochemistry of uranium in the Cariaco Trench. Bull. Mar. Sci. 21, 754–765.

Emerson, S.R., Huested, S.S., 1991. Ocean anoxia and the concentrations of molybdenum and vanadium in seawater. Mar. Chem. 34, 177–196.

Erickson, B.E., Helz, G.R., 2000. Molybdenum (VI) speciation in sulfidic waters: stability and lability of thiomolybdates. Geochim. Cosmochim. Acta 64, 1149–1158.

Fisher, I.St.J., Hudson, J.D., 1987. Pyrite formation in Jurassic shales of contrasting biofacies. In: Brooks, J., Fleet, A.J. (Eds.), Marine Petroleum Source Rocks. Geol. Soc. Lond., Spec. Publ., vol. 26, pp. 69–78.

Francois, R., 1988. A study on the regulation of the concentrations of some trace metals (Rb, Sr, Zn, Pb, Cu, V, Cr, Ni, Mn and Mo) in Saanich Inlet sediments, British Columbia, Canada. Mar. Geol. 83, 285–308.

Fry, B., Jannasch, H.W., Molyneaux, S.J., Wirsen, C.O., Muramoto, J.A., King, S., 1991. Stable isotope studies of the carbon, nitrogen and sulfur cycles in the Black Sea and the Cariaco Trench. Deep-Sea Res. 38, S1003–S1019 (Suppl.).

German, C.R., Elderfield, H., 1989. Rare earth elements in Saanich Inlet, British Columbia, a seasonally anoxic basin. Geochim. Cosmochim. Acta 53, 2561–2571.

German, C.R., Elderfield, H., 1990. Application of the Ce anomaly as a paleoredox indicator: the ground rules. Paleoceanography 5, 823–833.

German, C.R., Holliday, B.P., Elderfield, H., 1991. Redox cycling of rare earth elements in the suboxic zone of the Black Sea. Geochim. Cosmochim. Acta 55, 3553–3558.

Goldhaber, M.B., Kaplan, I.R., 1974. The sulfur cycle. In: Goldberg, E.D. (Ed.), The Sea, vol. 5. Wiley, New York, NY, pp. 569–655.

Haug, G.H., Pedersen, T.F., Sigman, D.M., Calvert, S.E., Nielsen, B., Peterson, L.C., 1998. Glacial/interglacial variations in production and nitrogen fixation in the Cariaco Basin during the last 580 kyr. Paleoceanography 13, 427–432.

Helz, G.R., Miller, C.V., Charnock, J.M., Mosselmans, J.F.W., Pattrick, R.A.D., Garner, C.D., Vaughan, D.J., 1996. Mechanisms of molybdenum removal from the sea and its concentration in black shales: EXAFS evidence. Geochim. Cosmochim. Acta 60, 3631–3642.

Huerta-Diaz, M.G., Morse, J.W., 1992. Pyritization of trace metals in anoxic marine sediments. Geochim. Cosmochim. Acta 56, 2681–2702.

Huffman Jr., E.W.D. 1977. Performance of a new carbon dioxide coulometer. Microchem. J. 22, 567–573.

Hughen, K.A., Overpeck, J.T., Peterson, L.C., Anderson, R.F., 1996a. The nature of varved sedimentation in the Cariaco Basin, Venezuela, and its palaeoclimatic significance. In: Kemp, A.E.S. (Ed.), Palaeoclimatology and Palaeoceanography from Laminated Sediments. Geol. Soc. Lond., Spec. Publ., vol. 116, pp. 171–183.

Hughen, K.A., Overpeck, J.T., Peterson, L.C., Trumbore, S., 1996b. Rapid climate changes in the tropical Atlantic region during the last deglaciation. Nature 380, 51–54.

Hughen, K.A., Overpeck, J.T., Lehman, S.J., Kashgarian, M., Southon, J., Peterson, L.C., Alley, R., Sigman, D.M., 1998. Deglacial changes in ocean circulation from an extended radiocarbon calibration. Nature 391, 65–68.

Hurtgen, M.T., Lyons, T.W., Ingall, E.D., Cruse, A.M., 1999. Anomalous enrichments of iron monosulfide in euxinic marine sediments and the role of H_2S in iron sulfide transformations: examples from Effingham Inlet, Orca Basin, and the Black Sea. Am. J. Sci. 299, 556–588.

Jacobs, L., Emerson, S., 1982. Trace metal solubility in an anoxic fjord. Earth Planet. Sci. Lett. 60, 237–252.

Jacobs, L., Emerson, S., Skei, J., 1985. Partitioning and transport of metals across the O_2/H_2S interface in a permanently anoxic basin: Framvaren Fjord, Norway. Geochim. Cosmochim. Acta 49, 1433–1444.

Jacobs, L., Emerson, S., Huested, S.S., 1987. Trace metal geochemistry in the Cariaco Trench. Deep-Sea Res. 34, 965–981.

Jones, B., Manning, D.A.C., 1994. Comparison of geochemical indices used for the interpretation of palaeoredox conditions in ancient mudstones. Chem. Geol. 111, 111–129.

Jørgensen, B.B., Weber, A., Zopfi, J., 2001. Sulfate reduction and anaerobic methane oxidation in Black Sea sediments. Deep-Sea Res. 48, 2097–2120.

Leventhal, J.S., 1983. An interpretation of carbon and sulfur relationships in Black Sea sediments as indicators of environments of deposition. Geochim. Cosmochim. Acta 47, 133–137.

Leventhal, J.S., 1987. Carbon and sulfur relationships in Devonian shales from the Appalachian Basin as an indicator of environment of deposition. Am. J. Sci. 287, 33–49.

Leventhal, J.S., 1995. Carbon–sulfur plots to show diagenetic and epigenetic sulfidation in sediments. Geochim. Cosmochim. Acta 59, 1207–1211.

Lewan, M.D., 1984. Factors controlling the proportionality of vanadium to nickel in crude oils. Geochim. Cosmochim. Acta 48, 2231–2238.

Lewan, M.D., Maynard, J.B., 1982. Factors controlling enrichment of vanadium and nickel in the bitumen of organic sedimentary rocks. Geochim. Cosmochim. Acta 46, 2547–2560.

Lewis, B.L., Landing, W.M., 1991. The biogeochemistry of manganese and iron in the Black Sea. Deep-Sea Res. 38, S773–S803 (Suppl.).

Lewis, B.L., Landing, W.M., 1992. The investigation of dissolved and suspended-particulate trace metal fractionation in the Black Sea. Mar. Chem. 40, 105–141.

Lin, S., Morse, J.W., 1991. Sulfate reduction and iron sulfide mineral formation in Gulf of Mexico anoxic sediments. Am. J. Sci. 291, 55–89.

Lin, H.-L., Peterson, L.C., Overpeck, J.T., Trumbore, S.E., Murray, D.W., 1997. Late Quaternary climate change from $\delta^{18}O$ records of multiple species of planktonic foraminifera: high-resolution records from the anoxic Cariaco Basin, Venezuela. Paleoceanograpy 12, 415–427.

Lyons, T.W., 1991. Upper Holocene sediments of the Black Sea: summary of Leg 4 box cores (1988 Black Sea Oceanographic Expedition). In: Murray, J.W., Izdar, E. (Eds.), Black Sea Oceanography. NATO Adv. Stud. Inst. Ser. Kluwer Academic Publishing, Dordrecht, pp. 401–441.

Lyons, T.W., 1992. Comparative study of Holocene Black Sea sediments from oxic and anoxic sites of deposition: geochemical and sedimentological criteria. PhD dissertation, Yale University, New Haven, CT. 377 pp.

Lyons, T.W., 1997. Sulfur isotopic trends and pathways of iron

sulfide formation in upper Holocene sediments of the anoxic Black Sea. Geochim. Cosmochim. Acta 61, 3367–3382.

Lyons, T.W., 2000. Iron/aluminum ratios: a new proxy for constraining depositional redox and sediment accumulation rates in ancient shale sequences. Abstr. Programs - Geol. Soc. Am. 32 (7), A289.

Lyons, T.W., Berner, R.A., 1992. Carbon–sulfur–iron systematics of the uppermost deep-water sediments of the Black Sea. Chem. Geol. 99, 1–27.

Middelburg, J.J., 1991. Organic carbon, sulphur, and iron in recent semi-euxinic sediments of Kau Bay, Indonesia. Geochim. Cosmochim. Acta 55, 815–828.

Middelburg, J.J., Calvert, S.E., Karlin, R., 1991. Organic-rich transitional facies in silled basins: response to sea-level change. Geology 19, 679–682.

Morse, J.W., Cornwell, J.C., 1987. Analysis and distribution of iron sulfide minerals in recent anoxic marine sediments. Mar. Chem. 22, 55–69.

Muller-Karger, F., Varela, R., Thunell, R., Scranton, M., Bohrer, R., Taylor, G., Capelo, J., Astor, Y., Tappa, E., Ho, T.-Y., Iabichella, M., Walsh, J.J., Diaz, J.R., 2000. Sediment record linked to surface processes in the Cariaco Basin. Eos (Trans. - Am. Geophys. Union) 81, 529 and 534–535.

Muramoto, J.N., Honjo, S., Fry, B., Hay, B.J., Howarth, R.W., Cisne, J.L., 1991. Fluxes of reduced sulfur, iron and organic carbon in the Black Sea using time-series sediment traps. Deep-Sea Res. 38, S1151–S1187 (Suppl.).

Newton, R.J., Bottrell, S.H., Dean, S.P., Hatfield, D., Raiswell, R., 1995. An evaluation of the use of the chromous chloride reduction method for isotopic analyses of pyrite in rocks and sediment. Chem. Geol. (Isot. Geosci. Sect.) 125, 317–320.

Passier, H.F., Middelburg, J.J., van Os, B.J.H., de Lange, G.J., 1996. Diagenetic pyritisation under eastern Mediterranean sapropels caused by downward sulphide diffusion. Geochim. Cosmochim. Acta 60, 751–763.

Passier, H.F., Middelburg, J.J., de Lange, G.J., Böttcher, M.E., 1997. Pyrite contents, microtextures, and sulfur isotopes in relation to formation of the youngest eastern Mediterranean sapropel. Geology 25, 519–522.

Peterson, L.C., Overpeck, J.T., Kipp, N.G., Imbrie, J., 1991. A high-resolution late Quaternary upwelling record from the anoxic Cariaco Basin, Venezuela. Paleoceanography 6, 99–119.

Peterson, L.C., Haug, G.H., Murray, R.W., Yarincik, K.M., King, J.W., Bralower, T.J., Kameo, K., Rutherford, S.D., Pearce, R.B., 2000. Late Quaternary stratigraphy and sedimentation at Site 1002, Cariaco Basin (Venezuela). In: Leckie, R.M., Sigurdsson, H., Acton, G.D., Draper, G. (Eds.), Proc. Ocean Drill. Program Sci. Results, vol. 165. Ocean Drilling Program, College Station, TX, pp. 85–99.

Raiswell, R., 1997. A geochemical framework for the application of stable sulphur isotopes to fossil pyritization. J. Geol. Soc. (Lond.) 154, 343–356.

Raiswell, R., Berner, R.A., 1985. Pyrite formation in euxinic and semi-euxinic sediments. Am. J. Sci. 285, 710–724.

Raiswell, R., Berner, R.A., 1986. Pyrite and organic matter in Phanerozoic normal marine shales. Geochim. Cosmochim. Acta 50, 1967–1976.

Raiswell, R., Canfield, D.E., 1996. Rates of reaction between silicate iron and dissolved sulfide in Peru Margin sediments. Geochim. Cosmochim. Acta 60, 2777–2787.

Raiswell, R., Canfield, D.E., 1998. Sources of iron for pyrite formation in marine sediments. Am. J. Sci. 298, 219–245.

Raiswell, R., Buckley, F., Berner, R.A., Anderson, T.F., 1988. Degree of pyritization of iron as a paleoenvironmental indicator of bottom-water oxygenation. J. Sediment. Petrol. 58, 812–819.

Raiswell, R., Whaler, K., Dean, S., Coleman, M.L., Briggs, D.E.G., 1993. A simple three-dimensional model of diffusion-with-precipitation applied to localised pyrite formation in framboids, fossils and detrital iron minerals. Mar. Geol. 113, 89–100.

Raiswell, R., Canfield, D.E., Berner, R.A., 1994. A comparison of iron extraction methods for the determination of degree of pyritisation and the recognition of iron-limited pyrite formation. Chem. Geol. 111, 101–110.

Raiswell, R., Newton, R., Wignall, P.B., 2001. An indicator of water-column anoxia: resolution of biofacies variations in the Kimmeridge Clay (Upper Jurassic, U.K.). J. Sediment. Res. 71, 286–294.

Repeta, D.J., 1993. A high resolution historical record of Holocene anoxygenic primary production in the Black Sea. Geochim. Cosmochim. Acta 57, 4337–4342.

Richards, F.A., 1975. The Cariaco Basin (Trench). Oceanogr. Mar. Biol. Ann. Rev. 13, 11–67.

Richards, F.A., Vaccaro, R.F., 1956. The Cariaco Trench, an anaerobic basin in the Caribbean Sea. Deep-Sea Res. 3, 214–228.

Schieber, J., Zimmerle, W., Sethi, P.S., 1998a. Shales and Mudstones, vol. 1. E. Schweizerbart'Sche Verlagbuchhandlung, Stuggart. 384 pp.

Schieber, J., Zimmerle, W., Sethi, P.S., 1998b. Shales and Mudstones, vol. 2. E. Schweizerbart'Sche Verlagbuchhandlung, Stuggart. 296 pp.

Scranton, M.I., Sayles, F.L., Bacon, M.P., Brewer, P.G., 1987. Temporal changes in the hydrography and chemistry of the Cariaco Trench. Deep-Sea Res. 34, 945–963.

Shipboard Scientific Party, P.G., 1997. Site 1002. In: Sigurdsson, R.M., Leckie, R.M., Acton, G.D., et al., (Eds.), Proc. Ocean Drill. Program, Initial Rep., vol. 165. Ocean Drilling Program, College Station, TX, pp. 359–373.

Sinninghe Damsté, J.S., Wakeham, S.G., Kohnen, M.E.L., Hayes, J.M., de Leeuw, J.W., 1993. A 6000-year sedimentary molecular record of chemocline excursions in the Black Sea. Nature 362, 827–829.

Spencer, D.W., Brewer, P.G., 1971. Vertical advection diffusion and redox potentials as controls on the distribution of manganese and other trace metals dissolved in waters of the Black Sea. J. Geophys. Res. 76, 5877–5892.

Sternbeck, J., Sohlenius, G., 1997. Authigenic sulfide and carbonate mineral formation in Holocene sediments of the Baltic Sea. Chem. Geol. 135, 55–73.

Sweeney, R.E., Kaplan, I.R., 1980. Stable isotope composition of dissolved sulfate and hydrogen sulfide in the Black Sea. Mar. Chem. 9, 145–152.

Taylor, S.R., McLennan, S.M., 1985. The Continental Crust: its Composition and Evolution Blackwell, Oxford. 312 pp.

Van Cappellen, P., Viollier, E., Roychoudhury, A., Clark, L., Ingall,

E., Lowe, K., DiChristina, T., 1998. Biogeochemical cycles of manganese and iron at the oxic–anoxic transition of a stratified marine basin (Orca Basin, Gulf of Mexico). Environ. Sci. Technol. 32, 2931–2939.

Werne, J.P., Hollander, D.J., Behrens, A., Schaeffer, P., Albrecht, P., Sinninghe Damsté, J.S., 2000a. Timing of early diagenetic sulfurization of organic matter: a precursor–product relationship in Holocene sediments of the anoxic Cariaco Basin, Venezuela. Geochim. Cosmochim. Acta 64, 1741–1751.

Werne, J.P., Hollander, D.J., Lyons, T.W., Peterson, L.C., 2000b. Climate-induced variations in productivity and planktonic ecosystem structure from the Younger Dryas to Holocene in the Cariaco Basin, Venezuela. Paleoceanography 15, 19–29.

Werne, J.P., Sageman,, B.B., Lyons, T.W., Hollander, D.J., 2002. An integrated assessment of a ''type euxinic'' deposit: evidence from multiple controls on black shale deposition in the Middle Devonian Oatka Creek Formation. Am. J. Sci. 302, 110–143.

Werne, J.P., Lyons, T.W., Hollander, D.J., Formolo, M.J., Sinninghe Damsté, J.S., 2003. Reduced sulfur in euxinic sediments of the Cariaco Basin: sulfur isotope constraints on organic sulfur formation. Chem. Geol. 195, 159–179 (this volume).

Wignall, P.B., 1994. Black Shales. In: Oxford Monographs on Geology and Geophysics. Oxford Univ. Press, New York. 127 pp.

Wignall, P.B., Meyers, K.J., 1988. Interpreting benthic oxygen levels in mudrocks: a new approach. Geology 16, 452–455.

Wignall, P.B., Newton, R., 1998. Pyrite framboid diameter as a measure of oxygen deficiency in ancient mudrocks. Am. J. Sci. 298, 537–552.

Wijsman, J.W.M., Middelburg, J.J., Heip, C.H.R., 2001. Reactive iron in Black Sea sediments: implications for iron cycling. Mar. Geol. 172, 167–180.

Wilde, P., Quinby-Hunt, M.S., Erdtmann, B.-D., 1996. The whole-rock cerium anomaly: a potential indicator of eustatic sea-level changes in shales of the anoxic facies. Sediment. Geol. 101, 43–53.

Wilkin, R.T., Arthur, M.A., 2001. Variations in pyrite texture, sulfur isotope composition, and iron systematics in the Black Sea: evidence for Late Pleistocene to Holocene excursions of the O_2–H_2S redox transition. Geochim. Cosmochim. Acta 65, 1399–1416.

Wilkin, R.T., Barnes, H.L., Brantley, S.L., 1996. The size distribution of framboidal pyrite in modern sediments: an indicator of redox conditions. Geochim. Cosmochim. Acta 60, 3897–3912.

Wilkin, R.T., Arthur, M.A., Dean, W.E., 1997. History of water-column anoxia in the Black Sea indicated by pyrite framboid size distributions. Earth Planet. Sci. Lett. 148, 517–525.

Wright, J., Schrader, H., Holser, W.T., 1987. Paleoredox variations in ancient oceans recorded by rare earth elements in fossil apatite. Geochim. Cosmochim. Acta 51, 631–644.

Yarincik, K.M., Murray, R.W., Lyons, T.W., Peterson, L.C., Haug, G.H., 2000a. Oxygenation history of bottom waters in the Cariaco Basin, Venezuela, over the past 578,000 years: results from redox-sensitive metals (Mo, V, Mn, and Fe). Paleoceanography 15, 593–604.

Yarincik, K.M., Murray, R.W., Peterson, L.C., 2000b. Climatically sensitive eolian and hemipelagic deposition in the Cariaco Basin, Venezuela, over the past 578,000 years: results from Al/Ti and K/Al. Paleoceanography 15, 210–228.

Zaback, D.A., Pratt, L.M., Hayes, J.M., 1993. Transport and reduction of sulfate and immobilization of sulfide in marine black shales. Geology 21, 141–144.

Zheng, Y., Anderson, R.F., van Geen, A., Kuwabara, J., 2000. Authigenic molybdenum formation in marine sediments: a link to pore water sulfide in the Santa Barbara Basin. Geochim. Cosmochim. Acta 64, 4165–4178.